UNIVERSITY OF MESSINA

DEPARTMENT OF ENGINEERING

Research Doctorate Course (D.M.45/2013)

"Engineering and Chemistry of Materials and Constructions"

XXXV Cycle

S.S.D. ING-IND/32

Development of reliability models for batteries in zero-emission powertrain

Ph.D. Candidate:
Salvatore Micari

PhD Coordinator:

Prof. Giovanni Neri

Tutor:
Prof. Salvatore De Caro

Co-Tutor (CNR-ITAE):
Ing. Laura Andaloro

_____

Anno accademico 2021-2022

Summary

1. Introduction

Environmental climate change has encouraged countries across the world to develop policies aimed to the reduction of energy consumption and greenhouse gas emissions. The introduction of Zero-Emission Vehicles based on electrical powertrains, could reduce the emission of environmental pollutants, the noise levels and could increase the liveability of urban areas. A progressive increment of the number of circulating EV is today observed worldwide, in fact in 2017 around 1.2 million were sold, with an increase of 57% compared to the previous year. China is today the country which produces the largest number of electric vehicles, followed by Europe, United State and Japan [P. di M. E-Mobility Report 2018. Energy&Strategy Group, School of Management, "Politecnico di Milano," 2018.]. The increase of electric vehicles using batteries will make this market a strategic one at global level. At least 30 million zero-emission electric vehicles are forecasted to be on EU roads by 2030. While electric cars are expected to significantly decrease greenhouse gas emissions, their batteries are harmful to the environment[1]. However, since today the dependence on oil and gas imports is still very high, just remember the increase in prices due to the conflict in Ukraine[2], the transition to a zero-emission economy will need to be combined with other energy vectors like hydrogen. An EV powertrain can feature different configurations, namely, full electric, parallel hybrid, series hybrid, power-split hybrid, but in any case, the battery is the main critical syste. The main components of a lithium-ion battery consist of two electrodes, a cathode and an anode, with a separator interposed between them, and a material, usually a solution, or an organic polymer, in which they are immersed, called electrolyte. The latter must be both electrically insulating and an excellent ionic conductor to easily transport lithium ions from one electrode to another. A lithium-ion battery should be able to provide a charge transfer reaction in order to reduce or oxidize the lithium ions, which can move and be inserted or released by electrodes during charge and discharge phases, in processes known as intercalation/deintercalation. Intercalation/deintercalation processes should be thermodynamically reversible and the electrochemical potential of cathode and anode should be inside the electrochemical stabilized window of the electrolyte [3]. The battery pack represents the container in which are contained the battery module, and this last one contained the electrochemical cells. However, the wide variety of chemical combinations between anode and cathode modify the performance and aging effects during use. Most commercially used LIBs can be divided based on cathode or anode technologies. The most common cathode materials are lithium nickel manganese cobalt oxide (NMC), lithium nickel cobalt aluminum oxide (NCA), lithium cobalt oxide (LCO), lithium manganese oxide (LMO), lithium nickel manganese oxide (LNMO), lithium iron phosphate

(LFP), lithium manganese iron phosphate (LMFP), lithium cobalt phosphate (LCP), while the anode materials are mainly graphite (C), silicon composite (Si/C) and lithium titanate oxide (LTO). The combinations are different, and the percentages of material used for cathodic or anodic combinations varies from manufacturer to manufacturer. The most common combinations are C/LCO, C/NMC, C/NCA, LTO/NMC, LTO/LMO, C/LNO, C/LMO, C/LFP [4]. Although in recent years research on batteries has brought several benefits to electric vehicle performance, key barriers to their adoption are still high cost, reduced autonomy, long charging times and the leak of a suitable network of charging stations. Substantial improvements in electric vehicles performance are expected with the development of new lithium-ion batteries, thanks to some notable advantages over other types of batteries, such as: high energy density, high power density, long cycle life and long calendar life. The battery pack design still representing an important challenge for Electric Vehicles (EVs) in terms of safety, reliability and system integration. For instance, overloading of the lithium-ion battery during adverse driving conditions can cause thermal runaway leading to serious fire hazards [5]-[6]. Thus, thermal management of the lithium-ion battery pack is crucial [7]. Moreover, the battery is subjected to ageing as effect of continuous charging and discharging cycles during its use. Similarly, the driver's driving style can age battery packs differently such us a ranged driving style with a higher frequency of power peaks than a cautious driving style [8].This will inevitably trigger an ageing process with the result of a loss of power and capacity that will progressively decrease over time. The degradation of the cells of a lithium-ion battery is the result of a complex interaction between different physical and chemical phenomena. This degradation phase affects the cells' ability to store energy and meet power requirements. The causes of failure are various and mainly depend on temperature, working conditions and time of use. The main aging mechanisms of lithium ion batteries are shown in Figure 1 through Ishikawa's diagram.
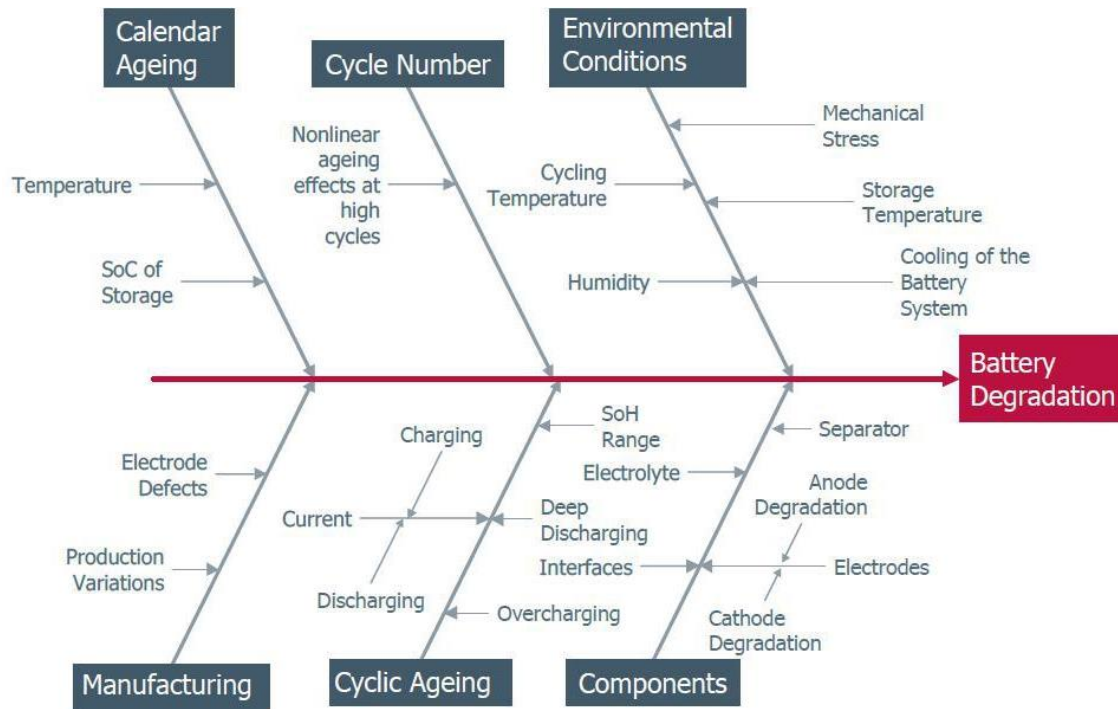
Figure 1: Ishikawa diagram of the main causes of aging of lithium-ion batteries.

The aging processes that occur at negative and positive electrodes differ significantly. The aging processes in the electrolyte and the separator result mostly, respectively, from reactions with the electrodes and reactions at the electrode-electrolyte interface [9]. The main degradation processes are SEI thickening when the battery cycling [10]-[11], deformation (volume change) and fracture/crack of electrode materials caused by diffusion induced stresses during cycling, which can result in short circuits that render electrode active materials incapable of storing lithium-ion [12]-[14], lithium plating [15]-[17]. At the positive electrode, the cathode, structural changes during the cycle, in combination with the chemical decomposition reactions of the electrode material, lead to a decrease in capacity and therefore a decrease in charge efficiency [9]. In addition, we can distinguish both calendar ageing, defined as the ageing to which the battery is subjected when it is not used, and cycle ageing like the ageing related to the use of the battery itself. Both types of aging depend on environmental conditions [18], state of charge [19], depth of discharge (DoD) [20]. The manufacturing aspects of the battery, i.e. variations in raw materials and assembly accuracy, complete the picture of relevant aging factors. Figure 2 shows a graphical syntesis the main degradation mechanisms that occur inside lithium-ion batteries.
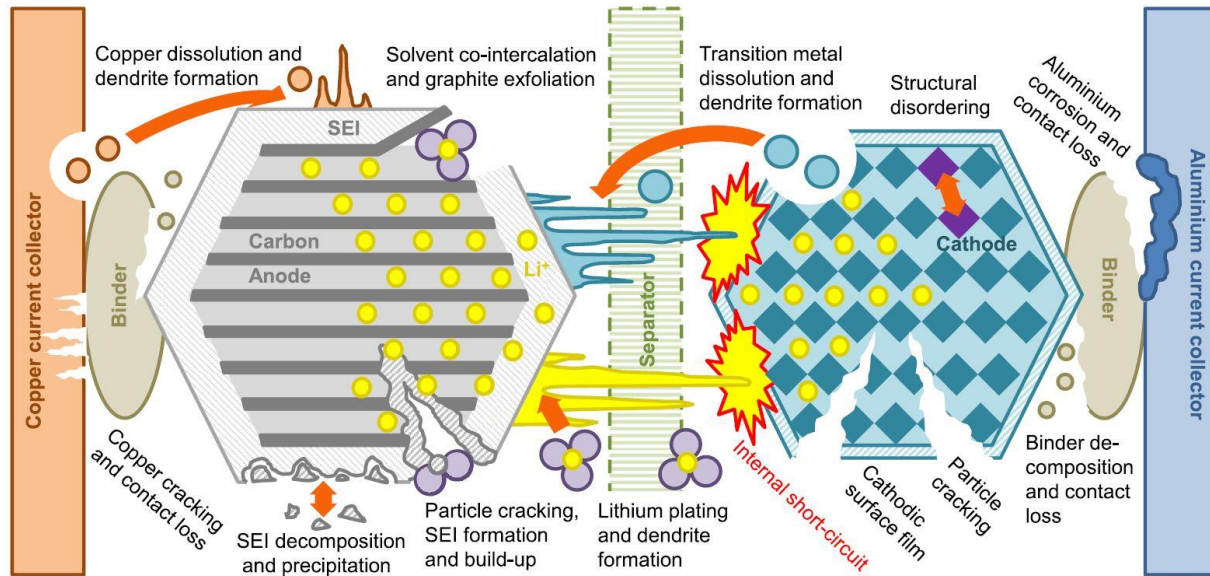
Figure 2: Mechanisms degradation in lithium-ion cells

These mechanisms can be grouped mainly in three macro areas listed below:

1. Loss of lithium inventory (LLI): lions are consumed by parasitic reactions such as: SEI (Solid Electrolite Interphase) formation, decomposition reactions, lithium plating. These are no longer available to be used for the intercalation/deintercalation reaction.

2. Loss of active material (LAM) at the anode: The active mass of the anode is no longer available for lithium insertion due to particle breakage and loss of electrical contact.

3. Loss of active material at the cathode: the active mass at the cathode is no longer available for lithium insertion due to structural disorders, cracking or loss of electrical contact.

These processes can lead to a capacity loss, power loss and an increase in internal resistance. The causes of failure are various and mainly depend on temperature and working conditions and time of use. Figure 3 shows the cause/effect relationship that causes lithium-ion batteries to age.
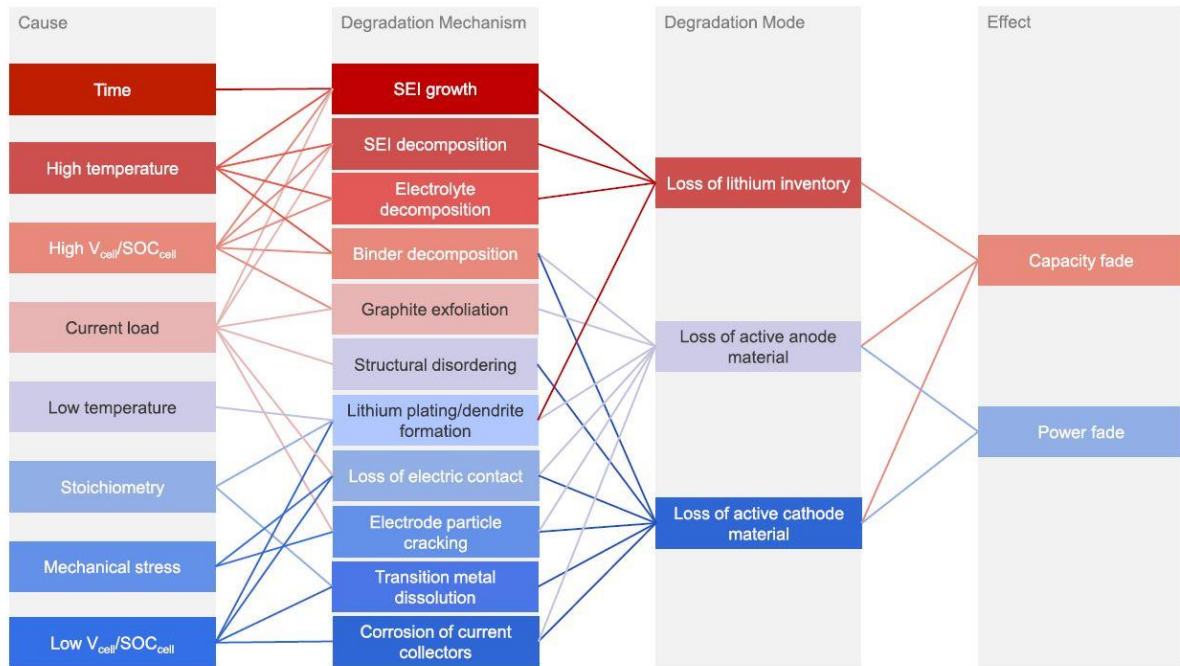
Figure 3: Relationship between cause and effect on battery degradation

In recent years, several studies have been carried out to evaluate the ageing of lithium-ion batteries. In [21] an important analysis of main ageing mechanisms occurring at anode, cathode, electrolyte and their interfaces is done with particular attention to carbonaceous anodes and some metal oxides cathodes, such as lithium manganese and lithium nickel-cobalt oxides. The paper describes the correlation of the causes (C-rate, temperature, DoD etc.) with various physical and chemical phenomena which are the reasons for performance degradation (capacity reduction, power fade, impedance variation). In particular, is underlined the importance of temperature both at high and low value as accelerating factor of ageing. An interesting and cited graphical synthesis, which summarize all the ageing mechanism inside a lithium battery, can be found in [22]. Therein, all the various degradation phenomena are clustered into three macro effects called degradation modes, which are respectively Loss of lithium Inventory (LLI), Loss of Active Material of the Negative Electrode (LAMNE), and Loss of Active Material of Positive Electrode (LAMPE). In case of LLI, some lithium ions become no longer available for charge/discharge processes due to parasitic reactions (i.e., Solid Electrolyte Interphase (SEI) growth, decomposition, lithium plating). The effect is a capacity fade but also, in case of film growth, a power fade. In LAMNE and LAMPE active masses, useful for

lithium ion insertion respectively in charge and discharge processes, become not useful due to particle cracking, loss of electrical contact, blocking of active sites, structural disordering. These processes happen in both the anode and cathode leading to capacity fade and power fade. In [23], after an introduction of main ageing mechanism affecting anode and cathode materials, two main types of ageing mechanisms were identified; calendar ageing, regarding the periods in which battery is unused, and cycle ageing, related to the application of the battery in real cases. In [24] a calendar and cycle ageing analysis is presented in terms of capacity fade and resistance increase for lithium-ion cells from different manufacturers. The cells were subjected to both calendar and cycle ageing, varying SoC and temperature in the former case and C-rate, DoD and temperature in the latter case. It is found that the temperature is the main parameter that affects the capacity fade and resistance increases for both calendar and cycle ageing [25]. Identifying the ageing of an electrochemical cell is particularly difficult to understand due to its nonlinear dependence on charge rate, state-of-charge and temperature [26].

Ph.D. focused on development of reliability models for batteries in zero-emission powertrain. The thesis reports the reliability models developed and the results obtained. An ageing model is then carried out able to describe the battery capacity loss, on the basis of environmental conditions and EV usage. This model is suitable to estimate the battery lifetime, residual capacity and reliability margins under different driving cycles, taking also into account the battery calendar ageing.

Most of the literature is focused on the investigation of degradation mechanisms under standard charge-discharge profiles. On the other hand, there is a lack of studies on the ageing mechanism induced by a real scenario, such as automotive application. The investigation conducted uses driving cycles that simulate a real automotive application in order to obtain valuable information for the evaluation of aging phenomena. In a first step the concept of evaluating the reliability of lithium-ion batteries for electric vehicles was explored. A mathematical model of the electric vehicle has been carried out to estimate the stress levels exerted to the battery during usage. A simple lithium ions battery model was used and improved with a lithium ion battery ageing model which estimates the loss of capacity due to cycling and calendar ageing. In a second step experimental tests are performed to investigate lithium-ion cell degradation under WLTP CLASS 3B driving cycle up to 10% capacity loss. The lithium-ion battery considered in this paper consists of a LMO-NMC cathode and a graphite anode with a capacity of 63Ah used in EV applications. The cell under test was aged at room temperature (25°C) for a number of cycles equal to 8 test years (4184 cycles) excluding calendar

ageing. IC and DV analysis were also performed to understand the evolution of the ageing process. From real data coming from WLTP CLASS 3B driving cycle a mathematical model for capacity loss from cycle ageing was extracted. Real data retrieved from a literature article [27] were analysed and a mathematical curve dependent on temperature and SOC was extracted to estimate the calendar ageing. Total ageing was computed as the sum of calendar and driving cycle contributions for 8 years and different Scenarios were then evaluated in order to predict the capacity loss.

2. EV lithium-ion Batteries reliability assessment

Operative temperature and electric current are crucial for the health of lithium-ion batteries. Overheating can accelerate the degradation of performances and heat excess can lead to a thermal runaway causing the disruption of the system and safety issues. Also, low temperatures can be critical during charge, due to lithium plating phenomenon with a consequent reduction of performances. Overcharge and over discharge heavily threat the health of lithium-ion batteries, in particular overcharge can be a triggering cause for thermal runaway. To face these issues lithium-ion battery packs are equipped with a Battery Management System (BMS) which manages charging/discharging processes and cell equalization, while controlling the temperature to avoid dangerous or unwanted operations. Although the BMS avoids the occurrence of potentially disruptive phenomena, performance degradation is however an unavoidable process, which is triggered by several factors, among them the internal battery temperature (Tbatt), the charge/discharge rate and the discharge depth. lithium-ion battery degradation is played in terms of both loss of capacity and drop of peak power. Capacity loss is due to transformation of active material into inactive phases, as a result of parasitic chemical reactions. Peak power reduction is caused by parasitic reactions, which convert battery materials into other compounds, which act as transport barriers, increasing the internal impedance. The decrease of battery capacity practically results in a shorter EV driving distance, while a peak power reduction influences the vehicle acceleration. A key role in developing operating strategies which can be exploited to reduce performance degradation of any system and to slow down ageing mechanisms is played by the reliability assessment [28]-[30]. The reliability of a battery is defined as the ability to hold its capacity above a given threshold after the expected lifetime. The goal of the reliability assessment of EV batteries is the estimation of the amount of driving cycles which the battery can support before losing a given percentage of its initial capacity. The reliability margin is then an evaluation of how many driving cycles the battery can withstand in excess to the number of driving cycles expected during the battery lifetime. The level of reliability of a battery can be estimated by mean of ageing mathematical models, which are able to predict from the results of laboratory tests the degradation of key battery parameters in practical operative conditions. Expected battery pack lifespan and the reliability margins can be estimated based on the following steps:

- Detection of main failure mechanisms.
- Development of an ageing model.
- Definition of the mission profile.
- Estimation of the expected lifespan.
- Evaluation of reliability margins.

A suitable procedure has been developed to assess the reliability of a lithium-ion battery for EV taking into account operating conditions. In fact, ageing and degradation mechanisms in EV batteries are heavily affected by working conditions. Tbatt is influenced by multiple factors including environmental temperature, heat generated. DOD, input/output current and SOC are related to EV operation, depending on trip distance and frequency of use, driver aggressiveness, acceleration, average and peak speed, road grade, etc. In addition, the SOC at which the battery is left when the EV is not used and the type of charging (regular, quick, very fast) could be very important ageing factors. According to Figure 4 a mathematical model of the electric vehicle first estimates the power stream exchanged between the battery and the electric powertrain during a specific driving cycle. This model consists of three main blocks namely: one dimensional dynamic model of the vehicle, AC motor model and inverter model [31]. For a given driving cycle the one-dimensional dynamic model of the vehicle first determines the traction effort on the basis of vehicle inertia, road grade, wheels rolling resistance and aerodynamic drag, then it computes the load torque at motor shaft Me* and shaft speed. The AC motor model in turn computes the electrical power Pme* which the inverter is tasked to provide. The model of the inverter finally estimates the power delivered by, or supplied to, the battery pack Pe*. The last is provided to a model of the battery which computes the stresses exerted to the battery in terms of charge/discharge C-rate, Tbatt and DOD. These represent the inputs of a battery ageing model, which estimates the loss of capacity due to cycling and calendar ageing.
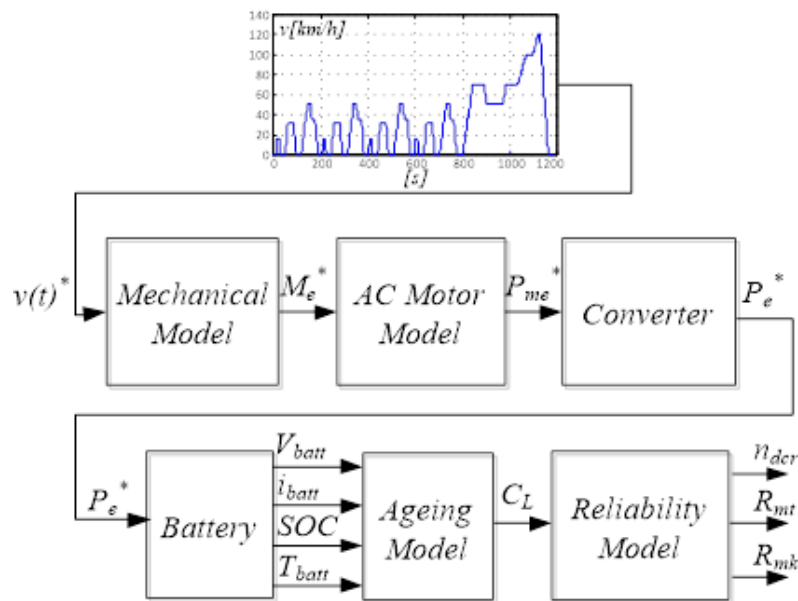

Figure 4: Block scheme of the reliability assessment procedure

The total loss of capacity per cycle, which is determined through the battery ageing model, is then processed to estimate the battery lifetime, residual capacity and reliability margins. By exploiting a cumulative stress approach, the total yearly capacity drop CLy can be computed by multiplying the capacity lost per cycle by the amount of driving cycles accomplished per day. The average capacity loss per cycle is then computed by dividing C_{Ly} by the total number of driving cycles ndc performed in one year:

$$\overline{C_L} = \frac{C_{Ly}}{n_{dc}} \qquad (1)$$

A 30% loss of the initial battery capacity is conventionally considered the maximum capacity drop allowed for batteries equipping electrical vehicles. The number of driving cycles which cause a 30% capacity loss is given by:

$$n_{dc-30\%} = \frac{0.3C_0}{\overline{C_L}} \qquad (2)$$

where C0 is the brand new battery capacity.

The residual number of driving cycles at time t is:

$$n_{dcr}(t) = n_{dc-30\%} - \frac{C_L(t)}{\overline{C_L}} \qquad (3)$$

being CL(t) the capacity lost up to time t.

The reliability margin can be computed either in terms of residual years of operation Rmt, either in terms of residual kilometers Rmk, before achieving a 30% reduction of the initial battery capacity:

$$R_{mt} = \frac{n_{dcr}}{\overline{n_{dc}}} \qquad (4)$$

$$R_{mk} = n_{dcr} \cdot l_{dc} \qquad (5)$$

During the third year of the PhD course, test on electrochemical cell for automotive applications was continued begun in the second year. The dynamic model for electric vehicles developed during the first two years of the research activity was used to extract from the WLTP CLASS 3B driving cycle the power profile to be applied to the cell under test. The dynamic model was calibrated to the characteristics of the BMW i3. Subsequently, tests were completed until an overall cell capacity loss of 10 percent from the initial capacity was achieved. Finally, test data were analysed in order to

understand degradation effects to identify capacity loss, resistance increase, and ageing phenomena using IC and DV curves. Finally, a mathematical model for capacity loss was extracted and the model was used to estimate battery ageing over possible vehicle operating scenarios. The experimental tests were performed thanks to C.N.R. I.T.A.E. (National Research Council - Institute of Advanced Technologies for Energy "Nicola Giordano") collaboration.

3. Lithium-ion battery model

According to Figure 4 a battery model is cascade connected to the vehicle model to provide the input for the ageing model. The mathematical model of the battery consists of two equations respectively dealing with discharge (6) and charge mode (7) temperature dependent from ambient temperature (T_a) compared to nominal ambient temperature (T_{ref}). The open circuit voltage and the polarization resistance are functions of the T_{batt} as well as of the actual battery capacity [32]. The considered battery model allows to compute the SOC and DOD from the battery current and capacity.

Discharge mode ($i^*>0$)

$$V_{batt} = E_0(T_{batt}) - \frac{K(T_{batt}) \cdot Q(T_a)}{Q(T_a) - i \cdot t}(i^* + i \cdot t) + Ae^{(-B \cdot i \cdot t)} - C \cdot i \cdot t - R(T_{batt})i \qquad (6)$$

Charge mode ($i^*<0$)

$$V_{batt} = E_0(T_{batt}) - \frac{K(T_{batt}) \cdot Q(T_a)}{i \cdot t + 0.1Q(T_a)}i^* - \frac{K(T_{batt}) \cdot Q(T_a)}{Q(T_a) - i \cdot t}i \cdot t + Ae^{(-B \cdot i \cdot t)} - C \cdot i \\ \cdot t - R(T_{batt})i \qquad (7)$$

where:

$$E_0(T_{batt}) = E_0(T_{ref}) + \frac{dE}{dT}(T_{batt} - T_{ref}) \qquad (8)$$

$$K(T_{batt}) = K(T_{ref}) \cdot e^{\alpha\left(\frac{1}{T_{batt}} - \frac{1}{T_{ref}}\right)} \qquad (9)$$

$$R(T_{batt}) = R(T_{ref}) \cdot e^{\beta\left(\frac{1}{T_{batt}} - \frac{1}{T_{ref}}\right)} \qquad (10)$$

$$Q(T_a) = Q(T_a) + \frac{\Delta Q}{\Delta T}(T_a - T_{ref}) \qquad (11)$$

$$SOC = 100\left(1 - \frac{1}{Q}\int_0^t i(t)dt\right) \qquad (12)$$

$$DOD = 100 - SOC$$

4. Preliminary lithium-ion battery ageing model

Ageing mechanisms of lithium-ion batteries mainly depend on the material used to build the cathode and anode and are different for each specific battery chemistry. The loss of capacity due to cycle ageing, which means the capacity drop due to normal battery operation is affected by the Tbatt, the rate of charge/discharge and the Depth of Discharge. A calendar ageing also occurs, dealing with degradation of the battery when it is not used, which is influenced by the ambient temperature [21].

Capacity drop caused by cycle ageing can be obtained as:

$$C_p = \frac{C_t \cdot F_{i-CD} \cdot F_{i-CC} \cdot F_{i-T} \cdot F_{i-DOD}}{n_t t_1} \tag{13}$$

where C_p is the capacity lost in one second, C_t is the capacity drop measured by through experimental tests after n_t t_l cycles each one taking t_l seconds, while $F_{i\text{-}CD}$, $F_{i\text{-}CC}$, $F_{i\text{-}T}$ and $F_{i\text{-}DOD}$ are acceleration factors respectively related to $C_{rate\text{-}c}$, $C_{rate\text{-}d}$, T_{batt} and DOD. According to previous literature [33]-[34], ageing factors are given by:

$$F_{i-DOD} = k_1(100 - DOD) + k_2 \tag{14}$$

$$F_{i-T} = k_3 \cdot e^{k_4 \cdot T_{batt}} \tag{15}$$

$$F_{i-CC} = k_5 \cdot \left| C_{rate-c}^{k_6} \right| \tag{16}$$

$$F_{i-CD} = k_7 \cdot e^{k_8 \cdot |C_{rate-d}|} \tag{17}$$

where k_i are coefficients which are specific for the considered battery. The coefficients of the ageing factor $F_{i\text{-}DOD}$ have been obtained from the SOC curve by considering that *SOC = 1 – DOD*. The coefficients of the other ageing factors were instead obtained by combining some diagrams provided by the battery manufacturer with information deducted from [33]-[35].

Capacity reduction due to calendar ageing is affected only by the T_{batt}, which fairly coincides with the T_a. An Arrhenius kinetics model is used to deal with calendar ageing [36], given by:

$$C_c(t) = h_1 e^{-\left(\frac{h_2}{T_{batt}}\right)} + h_3 \tag{18}$$

where C_c is the battery capacity lost at time *t* due to calendar ageing and h_1, h_2 and h_3 are coefficients which are specific for the considered battery. All the coefficients needed by functions used for developing the model were extracted by using MATLAB interpolation tool, implementing formula, data and variable inside the tool.

4.1. EV driving cycles profiles

Main features of the considered electrical vehicle are shown in Table 1

Table 1: Electric Vehicle technical specifications extrapolated from Technical specifications of BMWi3 model [37]

Vehicle Type	Battery Electric vehicle (BEV)
Vehicle mass	1195 kg
Frontal area	2,8 m^2
Drag coefficient	0,29
Rolling friction coefficient	0,012
Transmission gear ratio	9,7
Hub diameter	48 cm
Tire width	15,5 cm
Tire aspect ratio	70 %
Wheel radius	25,4 cm
Motor type	AC - PMSM
Motor rated power	75 kW
Motor rated speed	4800 rpm
Motor pole pairs	4
Battery pack	85 cells in series

Some different driving cycles can be taken as reference for lithium-ion batteries reliability assessment. The New European Driving Cycle (NEDC), shown in Figure 5 considers typical driving conditions in Europe and consists of four urban driving cycle (UDC) and one extra urban driving cycle (EUDC). The distance covered is 10.93 km in 1180 s, achieving a maximum speed of 120 km/h. The World harmonized Lightduty vehicles Test Procedure (WLTP) deals with three different driving profiles, each one dealing with a specific vehicle class (1: low power, 2: medium power, 3: high power). In particular: WLTP Class 1 driving cycle covers a distance of 8091 km in 1022 s with a maximum speed of 65 km/h as shown in Figure 6. WLTP Class 2 driving cycle deals with a distance of 14664 km covered in of 1477 s with a maximum speed of 85 km/h as shown in Figure 7. Finally, WLTP Class 3B considers a distance of 23266 km to be covered in 1800 s with a peak speed of 131.3 km/h, as shown in Figure 8.
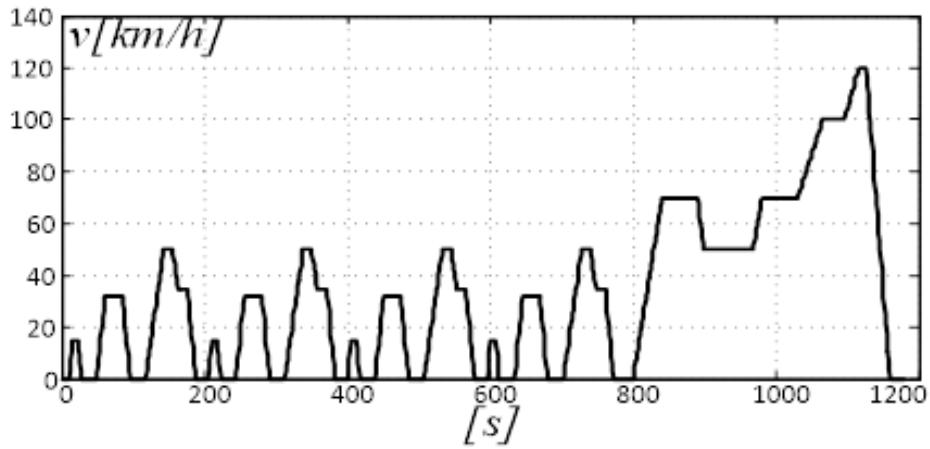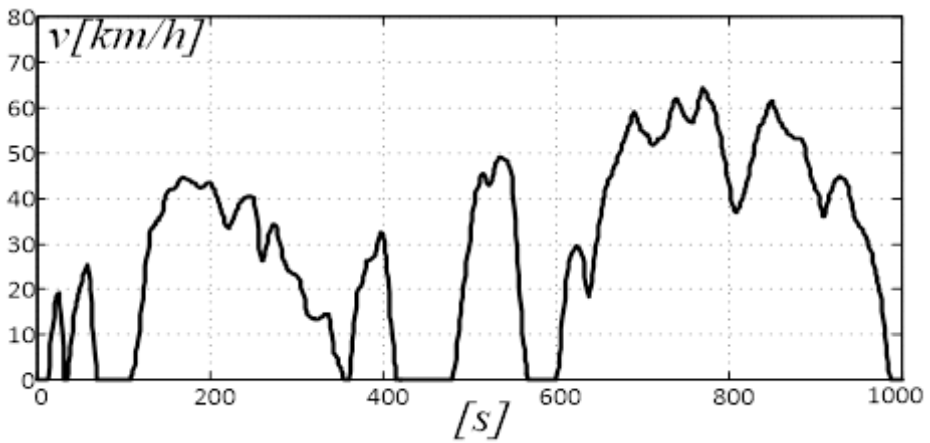
Figure 5: NEDC driving cycle

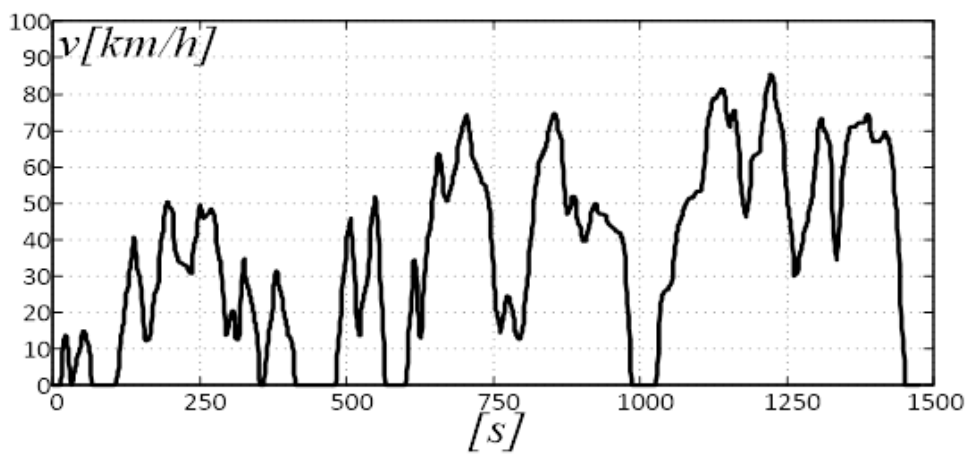Figure 6: WLTP CLASS 1 driving cycle

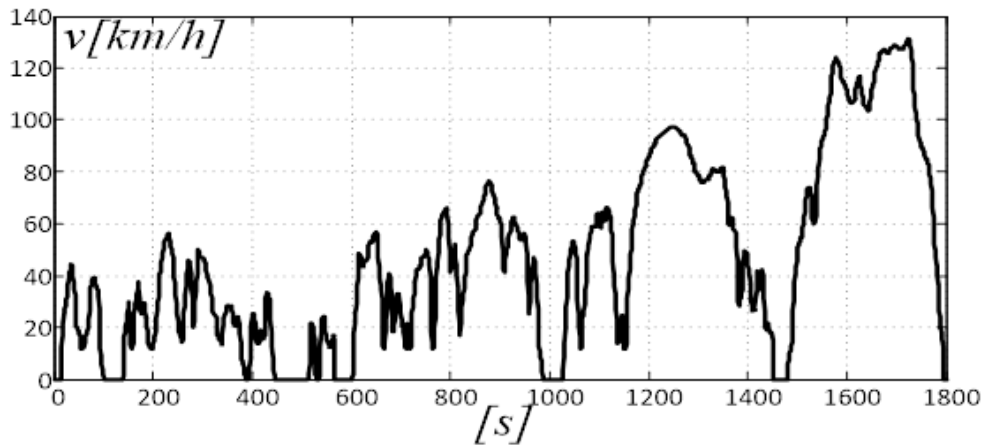
Figure 7: WLTP CLASS 2 driving cycle

Figure 8: WLTP CLASS 3B driving cycle

In order to define the number of daily driving cycles to consider, average data about the distance traveled in Europe per weekday and weekend have been used [38] In detail, the average distance covered in a weekday is 32.8 km, the distance covered in a weekend of two days is 34.6 km per day. Assuming a typical year composed by 261 weekdays, and 52 weekends, the total distance covered in a year is about 8561 km on weekdays and 3598 km on weekends, for a total of 12159 km. The assumptions shown in Table 2 are done in order to cover the average daily distance by using the considered standard driving cycles. A degradation figure often used for EV batteries warranty is to reach a 70% residual capacity after 8 years or 160000 km (100000 mi) usage.

Table 2: Typical yearly vehicle utilization

	Weekdays	Driving cycles per day	Weekend	driving cycles per day
NEDC (10930 km)	261	3	87	3
			17	4
Yearly distance	8558 km		3596 km	
WLTP CL. 1 (8091 km)	247	4	75	4
	14	5	29	5
Yearly distance	8560 km		3600 km	
WLTP CL. 2 (14664 km)	199	2	67	2
	62	3	37	3
Yearly distance	8563 km		3593 km	
WLTP CL. 3B (23266 km)	154	1	53	1
	107	2	51	2
Yearly distance	8562 km		3606 km	

4.2. Ageing model tuning and validation

The lithium-ion battery for Electric Vehicles applications [39] considered in this paper, hereafter referred as Device Under Test (DUT), consists of a LMO-NMC cathode and a graphite anode with a capacity of 63Ah, whose technical specifications are given in Table 3.

Table 3: Lithium-ion battery technical specifications from datasheet

	Cell Type	Lithium-ion
	Chemistry Cathode	LMO-NMC
	Chemistry Anode	Graphite
	Capacity	63 Ah
	Nominal voltage	3,75 V
	Operating voltage	2,7 V-4,12 V
	Battery temperature	-40-65 °C
Discharge	Continuous 25°C	120 A
Charge	Continuous 25°C	150 A
Cycle life	25°C, EOL80% / EOL 70%	3200 / 5200
	45°C, EOL80% / EOL 70%	1500 / 2500
Calendar life	SOC100%, 25°C, EOL80% / EOL 70%	17 / 26 years
	SOC100%, 60°C, EOL80%	3.5 years

Discharge characteristics of a battery pack composed of 85 of these batteries are shown in Figure 9.
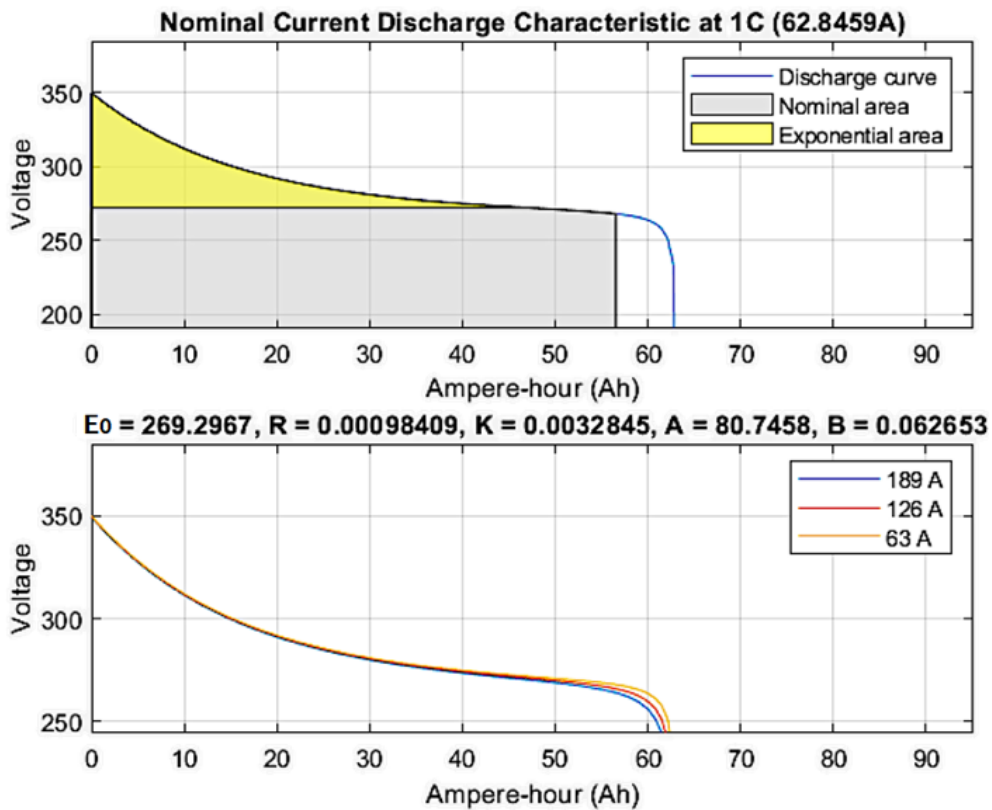
Figure 9: Battery discharge diagrams.

Coefficients of cycle ageing acceleration factors have been obtained by best fitting eqs (14)-(17) with information provided by the battery datasheet, containing an exhaustive set of test results, base characterizations, performance tests and ageing graphs at different conditions. The obtained coefficients are given in Table 4, while accelerating factors are plotted in Figure 10.

Table 4: Coefficients of acceleration factors

k_1	0.001
k_2	0.9
k_3	0.0368
k_4	0.04
k_5	1.186
k_6	0.2145
k_7	0.8612
k_8	0.1547

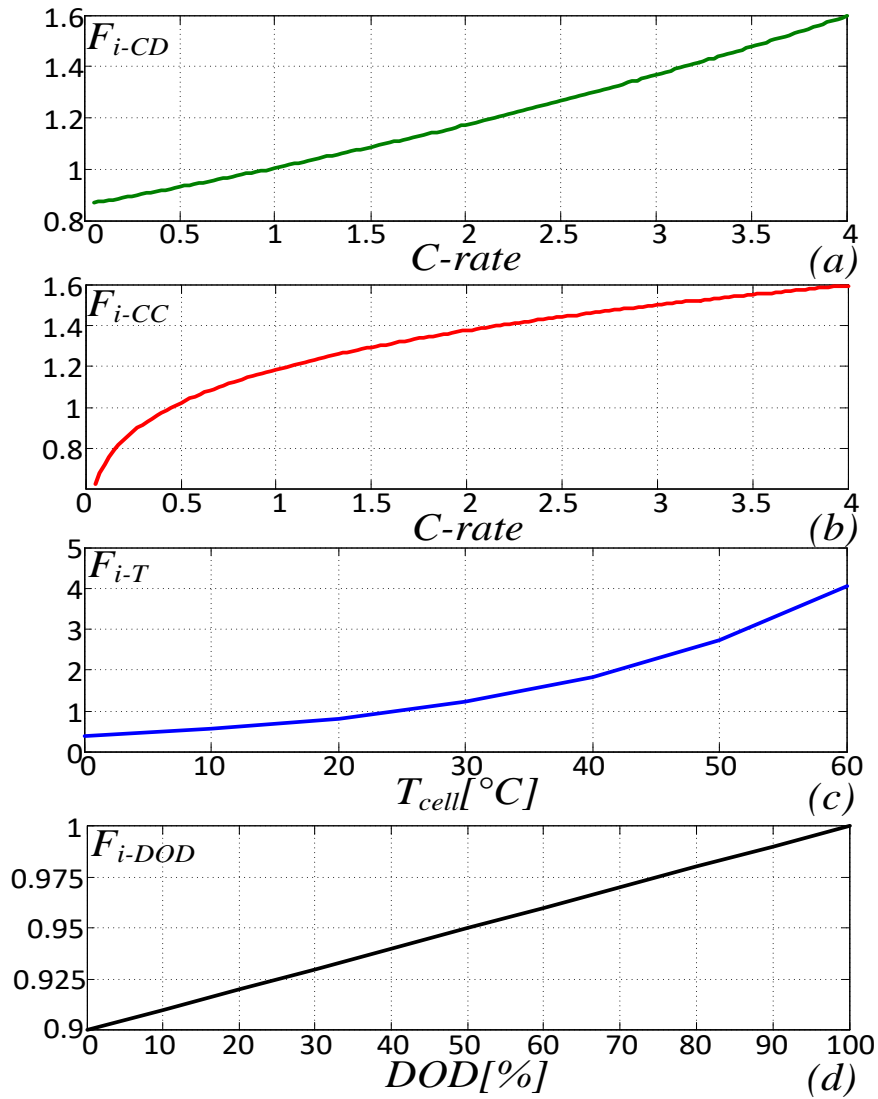Figure 10: Acceleration factors diagrams.

Coefficients of (18) have been found from battery datasheet on calendar like reported in Table 3. The coefficient data are reported in Table 5 and a plot of the battery calendar ageing decay is provided in Figure 11.

Table 5: Coefficients of calendar ageing equation

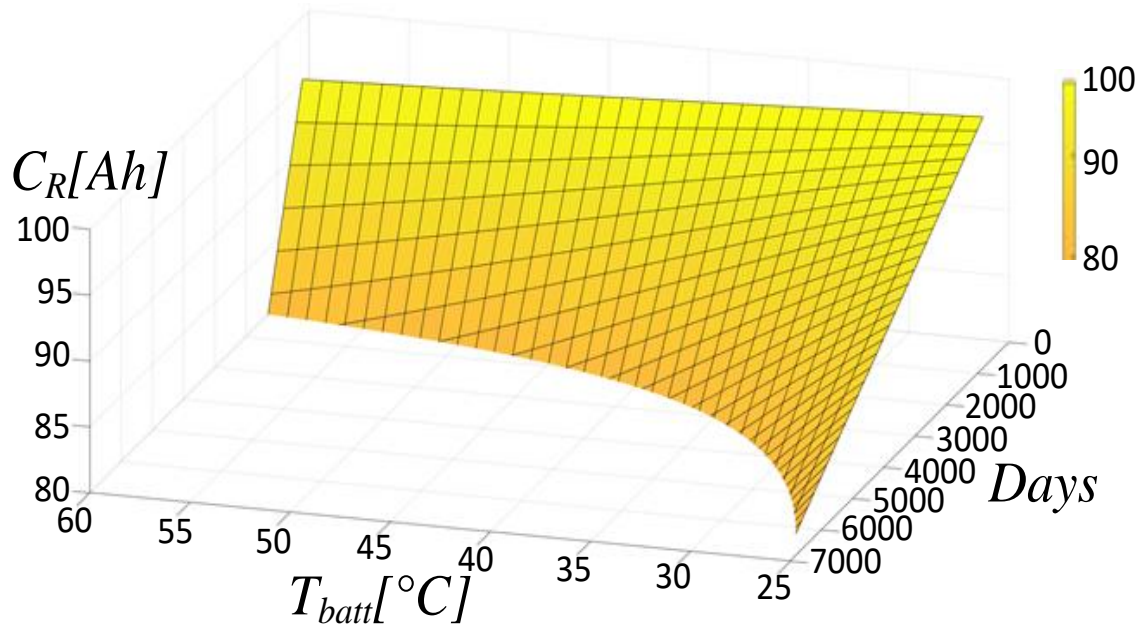|	
h_1	-0.046
h_2	71.8
h_3	98

Figure 11: Calendar ageing decay.

4.3. Reliability margins computation

A simulation dealing with the considered electric vehicle accomplishing a WLTC Class 3B driving cycle is shown in Figure 12 and Figure 13.
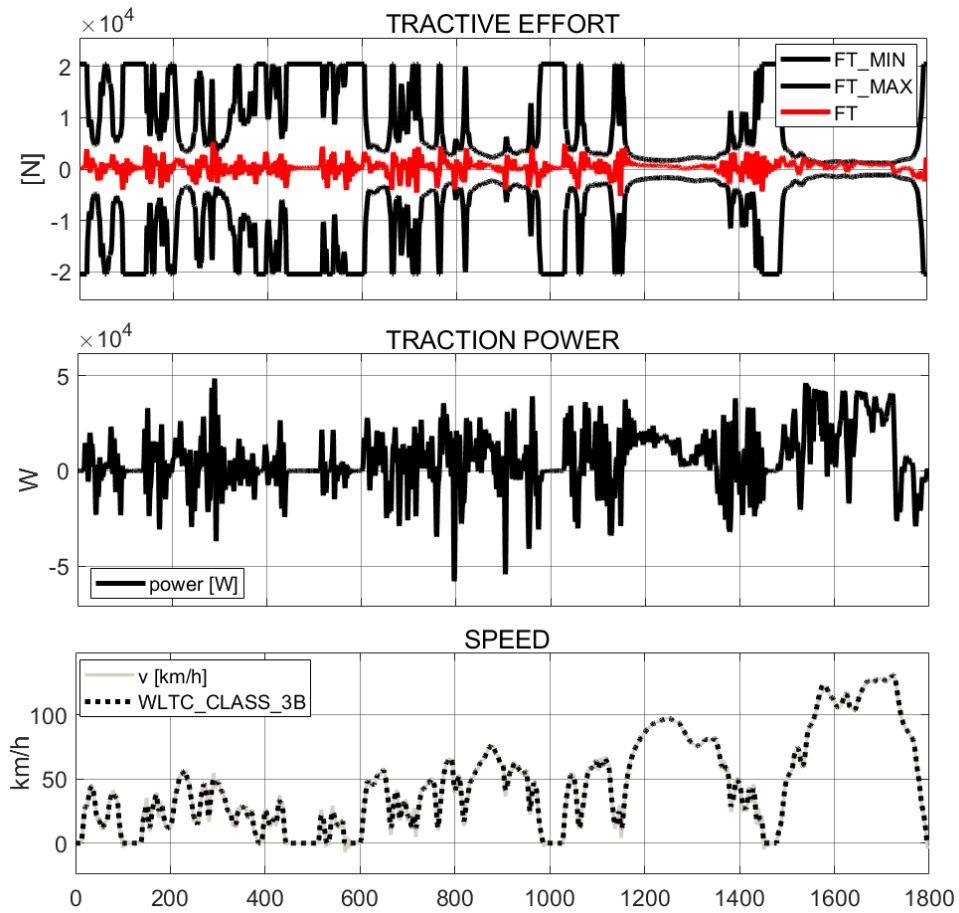

Figure 12: WLTC CLASS 3B vehicle simulation
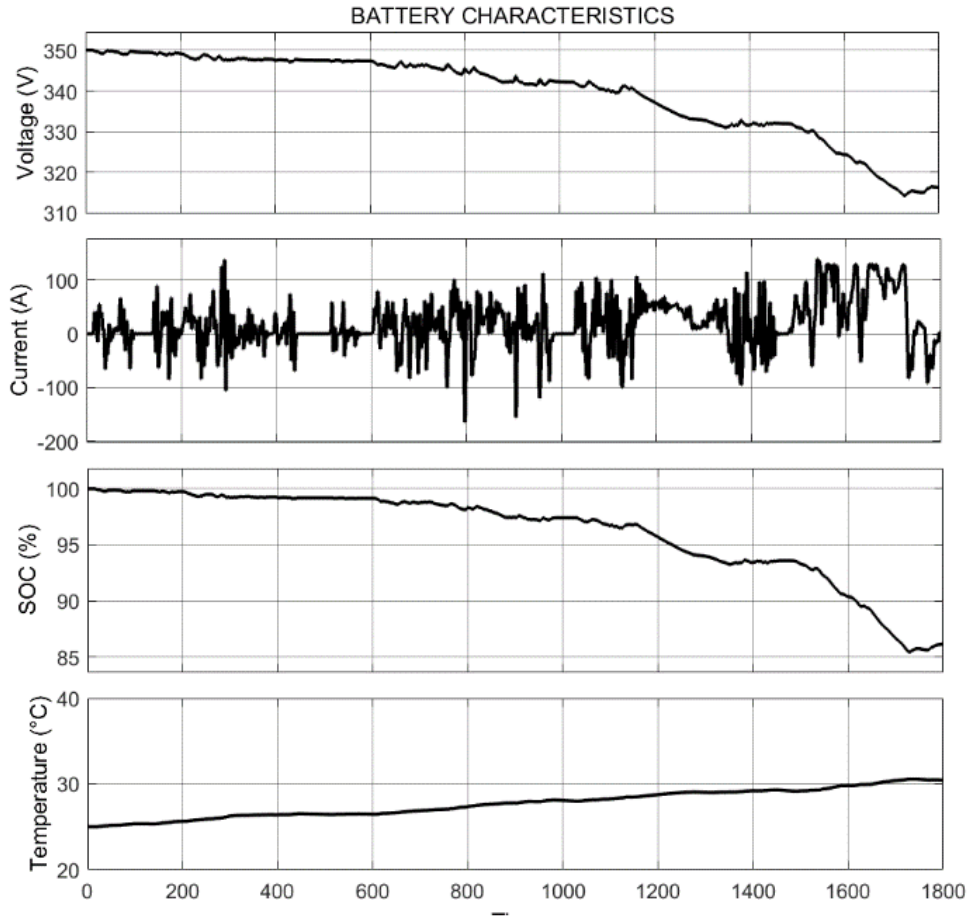
Figure 13: WLTC CLASS 3B battery simulation.

The total capacity lost after *t* seconds is given by:

$$C_L(t) = \sum_{k=0}^{t} \left[C_p(k) + C_c(k) \right] \tag{19}$$

where $C_p(k)$ and $C_c(k)$ are the values of the capacity lost respectively for cycle and calendar aging in the *k-th* second of the simulation, according to (13) and (18). The battery residual capacity at time *t* is then computed as:

$$C_r(t) = C_0 - C_L(t) \tag{20}$$

The residual battery capacity after a day of operation is computed from (20) for a given driving cycle. The residual battery capacity after some years of operations has been then computed according to Table 2, as shown in Table 6.

Table 6: Residual capacity estimation

Vehicle age	NEDC ($n_{dcy}=1112$)	WLTP CL. 1 ($n_{dcy}=1503$)	WLTP CL. 2 ($n_{dcy}=829$)	WLTP CL. 3B ($n_{dcy}=524$)
Brand new	100	100	100	100
1 year	97.6899	98.2503	97.9262	99.5003
2 years	95.3791	96.5003	95.8518	99.006
3 years	93.0677	94.75	93.777	98.3152
4 years	90.7555	92.9993	91.7017	97.550
5 years	88.4425	91.2484	89.6257	93.5778
6 years	86.1289	89.497	87.5493	92.2931
7 years	83.8143	87.7455	85.4723	91.0085
8 years	81.4991	85.9934	83.3947	89.7238
9 years	80	84.241	81.3164	88.4391
10 years		82.4883	79.2373	87.1545

Residual number of driving cycles after 8 years are shown in Table 7. Expected distance covered by the vehicle before losing 30% of the initial battery capacity is shown in Table 8, while reliability margin and extra distance to travel are shown in Table 9 and Table 10.

Table 7: Residual number of driving cycles.

Vehicle age	NEDC ($n_{dcy}=1112$)	WLTP CL. 1 ($n_{dcy}=1503$)	WLTP CL. 2 ($n_{dcy}=829$)	WLTP CL. 3B ($n_{dcy}=524$)
Brand new	9627	17180	7995	8145
1 year	8512	15674	7164	7621
2 years	7398	14168	6333	7099
3 years	6283	12661	5502	6574
4 years	5167	11156	4671	6051
5 years	4053	9648	3840	5527
6 years	2937	8144	3009	5005

7 years	*1822*	*6636*	*2177*	*4481*
8 years	*722*	*5130*	*1346*	*3958*
9 years		*3624*	*526*	*3436*
10 years		*2136*		*2913*

Table 8: Expected traveled distance before losing 30% of C0.

NEDC	*105223 km*
WLTP CLASS 1	*139003 km*
WLTP CLASS 2	*117239 km*
WLTP CLASS 3B	*189502 km*
Average	*137742 km*

Table 9 Reliability margin to 8 years operational life.

NEDC	*237d*
WLTP CLASS 1	*2y 153d*
WLTP CLASS 2	*1y 232d*
WLTP CLASS 3B	*7y 208d*
Average	*3y 25d*

Table 10: Expected extra distance to travel

NEDC	*7880 km*
WLTP CLASS 1	*41506 km*
WLTP CLASS 2	*19737 km*
WLTP CLASS 3B	*92086 km*
Average	*40303 km*

Taking into account the considered driving cycles, reliability margin is always greater than zero, hence the considered battery pack is suitable to ensure an 8 years operational life. However, a second warranty limit is often also set for EV batteries, consisting in a minimum 160000 km distance traveled before reaching 70% of the initial battery capacity. Considering this limit, the reliability margin in

terms of kilometers to be traveled is negative, as shown in Table 11, which means that the considered battery pack is unsuitable to fulfill the given mission.

Table 11: Reliability margin to 160000 km

NEDC	*-14740 km*
WLTP CLASS 1	*-35617 km*
WLTP CLASS 2	*-9606 km*
WLTP CLASS 3B	*-8794 km*
Average	*-17189 km*

The developed procedure can be exploited to evaluate the effectiveness of any kind of measure intended to extend the battery lifetime. These measures may deal with increasing the inverter DC-bus capacitance, introducing a supercapacitor in parallel to the batteries or by increasing the number of series connected batteries. Moreover, optimal management of charging, for example decreasing the C-rate during overnight recharge could attenuate the effect of ageing. The estimation of the residual capacity of an EV battery at the end of its operative life is also an important issue for possible further uses. In fact, they still feature up 80% of residual capacity, making possible their reuse in applications less demanding than EV, such as stationary energy storage systems, where they could represent a low-cost alternative to brand new batteries [40].

Obtained results in terms of residual battery capacity can also be exploited to estimate the range achievable by a vehicle having an aged battery. A comparison between the distance covered by a vehicle equipped with a brand new battery and a vehicle with a 4 years old battery is shown in Fig. 21. In both cases, the initial SOC is 100% and the battery voltage is about 350V. Assuming a residual 20% SOC in the two cases, the vehicle with the 4 years old battery features 30 km less.
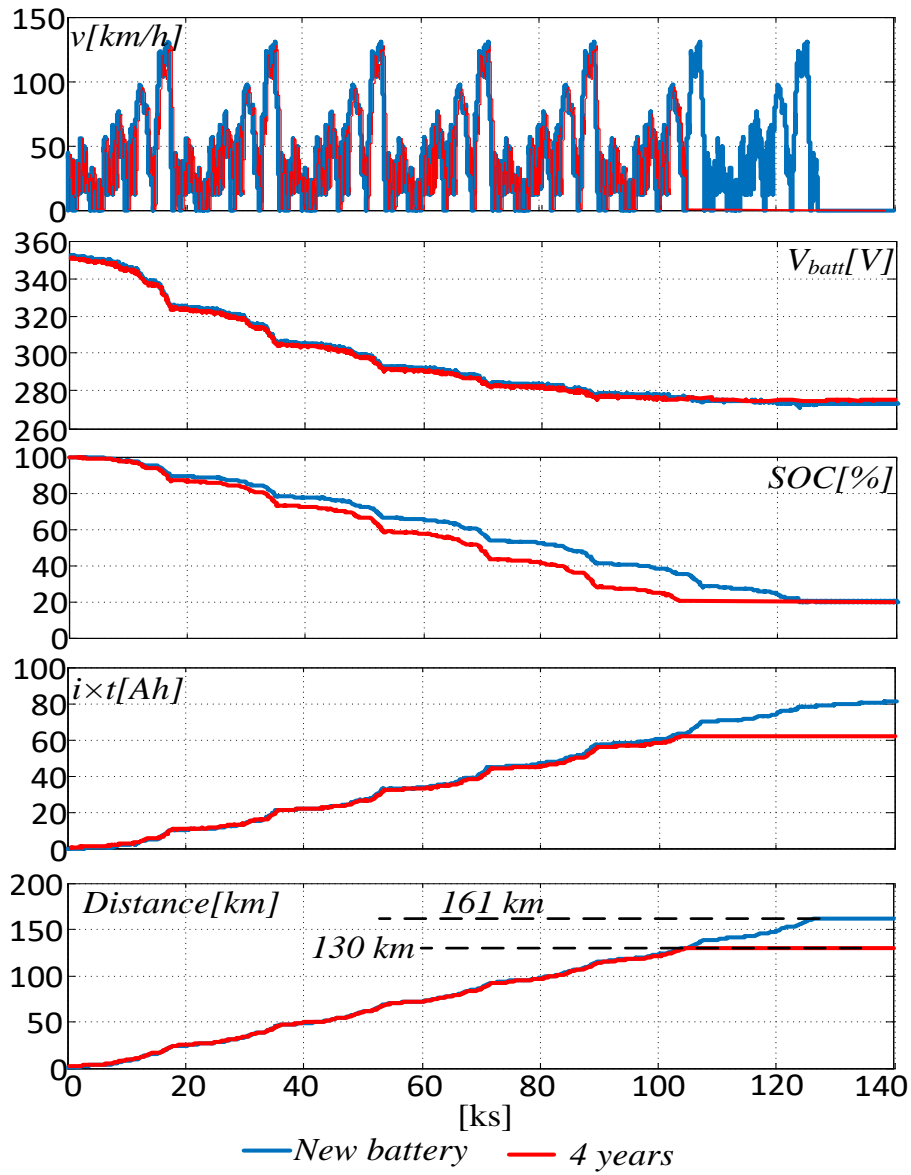
Figure 14: WLTC CLASS 3B: Performance of a vehicle with a brand new battery and a vehicle with a four years old battery.

5. Lithium-ion cell ageing test procedures

5.1. EV mission profile

The World harmonized Light duty vehicles Test Procedure (WLTP) is a globally harmonized standard for determining levels of pollutants such as CO_2. It is used for fuel consumption of internal combustion engines (ICE) and to determine the range of electric vehicles.

The WLTP procedures include several World harmonized Light duty vehicle Test Cycles (WLTC) for different categories of vehicles based on the power-to-mass ratio (PMR), defined as the ratio of rated power (W) to ground mass (kg) (excluding driver), and the maximum speed (vmax) of the vehicle as declared by the automaker. It includes three different WLTC test cycles, depending on the class of vehicle according to PMR:

- Class 1 - low power vehicles with PMR ≤ 22;

- Class 2 - vehicles with 22 < PMR ≤ 34;

- Class 3 - high-power vehicles with PMR > 34;

The work is focused on high-power vehicles. Therefore, it was chosen to perform the tests using the WLTP CLASS 3B cycle. The WLTP 3b cycle is composed of four sections: low, medium, high, and extra high. For our purposes, the WLTP CLASS 3B was selected with a length of 23,266 km to be covered in 1.800 s with a peak speed of 131,3 km/h, as shown in Figure 15. Each part contains a variety of driving phases, stops, acceleration and braking phases. Usually, the four phases are associated with a high traffic density urban road for the low part, a low traffic density urban road for the medium part, a suburban road for the high part, and a highway road for the extra high part [41].
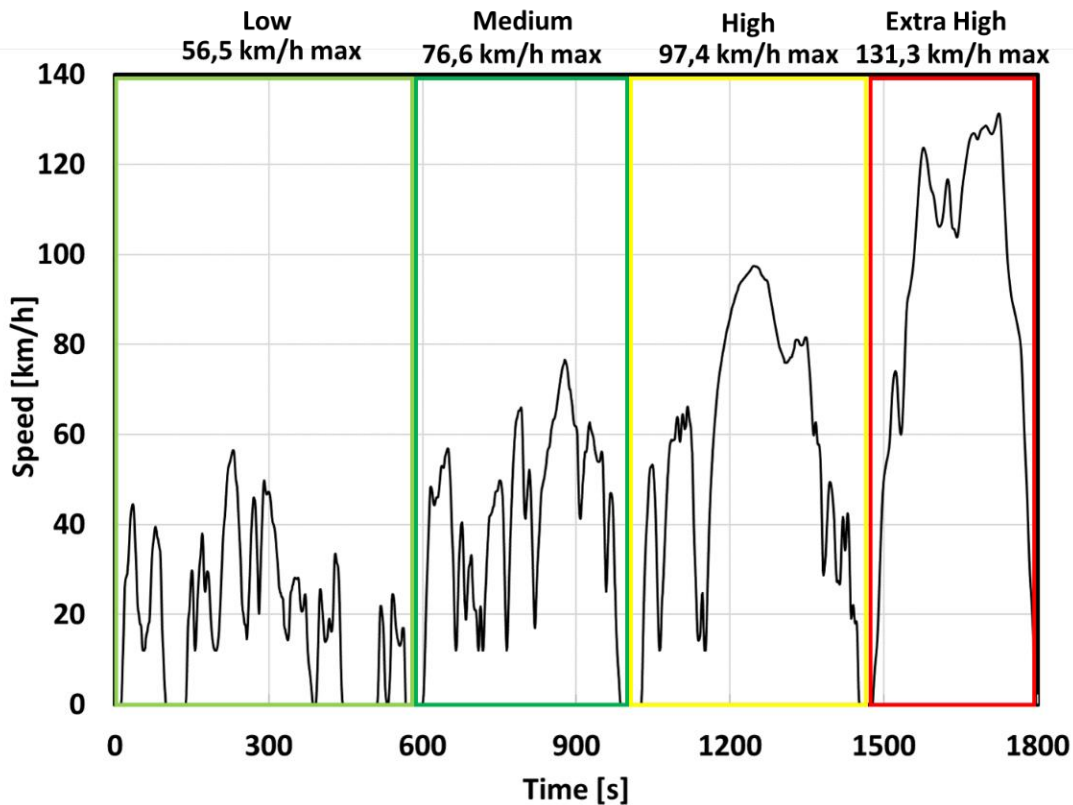
Figure 15: Worldwide harmonized Light vehicles Test Procedure 3B for determining energy consumption for light duty electric vehicles with power-to-weight ratio greater than 34 (WLTP CLASS 3B driving cycle).

The driving cycle is defined in terms of speed and time. To identify the power profile required for the cell under test the vehicle model proposed in [42] was used and depicted in Figure 4. After verifying that the driving cycle used was correctly reproduced from the model, as shown in Figure 16, the battery current profile was extracted through the model and applied to a single electrochemical cell. The current profile was used instead of the power profile because the software for automatic creation of the cycler program did not support this option.

Since the SOC, it was found useful to limit the SOC of the cell under test to 30% maximum, furthermore for the current profile extraction has been used the nominal voltage matching with 50% SOC. Under these conditions, the operating voltage window is relatively close to the nominal value of 3,75 V. As a result, the error between the current profile extracted from the model and the current profile computed as the ratio of power and rated voltage of 3,75V have a max error of 13,36% and a mean error of 7,78% (Figure 17). The error was deemed acceptable.
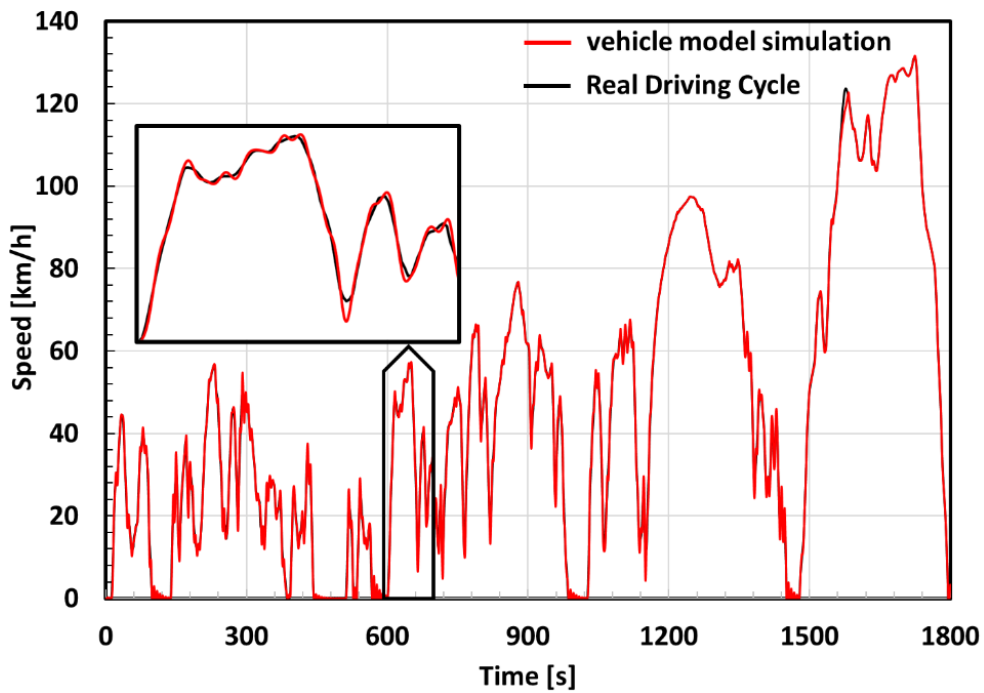
Figure 16: Comparison between WLTP CLASS 3B driving cycle and vehicle model simulation
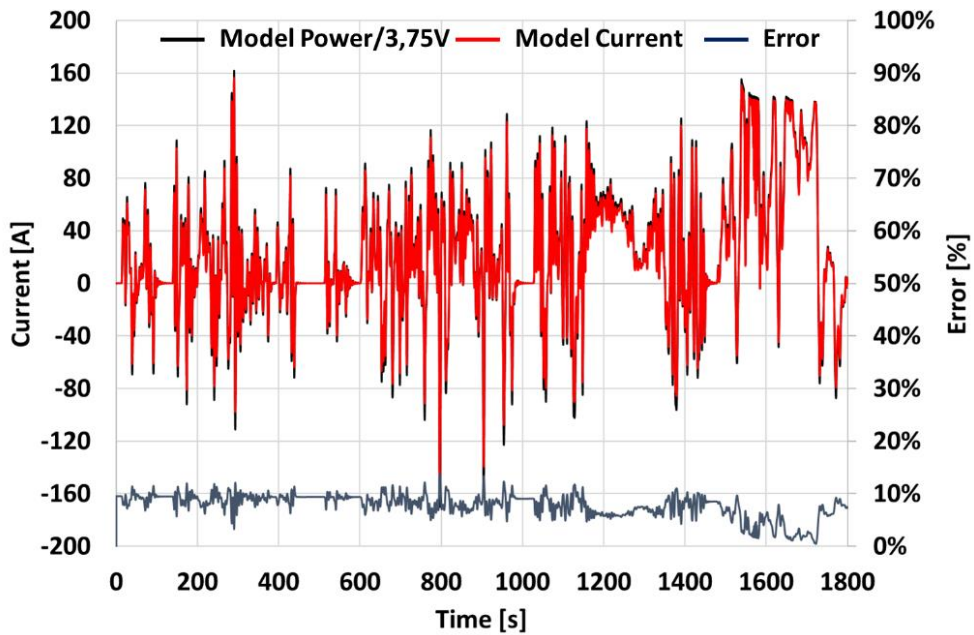
Figure 17: Battery current computed as the ration of power on rated voltage and error.

To correlate the number of driving cycles and vehicle operating times, average data of distance driven in Europe by a light duty vehicle were taken as reference [38]. The total distance is 12.168,12 km, equivalent to 523 driving cycles per year. The tests were then carried out in steps of 261/262 driving cycles before checking the characteristics of the DUT.

5.2. Test procedures

A prismatic lithium-ion battery cell was used to investigate the effect of WLTP CLASS 3B driving cycles. The cell is aged with WLTP CLASS 3B driving cycle at ambient temperature (25°C) for a number of cycles equal to 8 real years (4184 cycles) neglecting calendar ageing (test years). The sequence of cycles involves the electrochemical cell recharging at 1C when the voltage reaches 3,1V. After the cell has reached the upper cut off voltage of 4,12V, the cycle continues from where it had stopped. Suitable tests are accomplished at the beginning of the ageing test and every 261/262 cycles to verify the characteristics of the cell under test. These are a capacity test (Figure 18) and a pulse test (Figure 19).

The capacity test is performed to verify the capacity of the cell. It consists of 3 complete charge and discharge cycles within the upper and lower cut off voltage of 4,12 V and 2,7 V, respectively, at Constant Current (CC) for the discharge and Constant Current-Constant Voltage (CC-CV) for the recharge at 25°C. This procedure, which is performed to stabilize the active materials of the cells is described in Table 12.
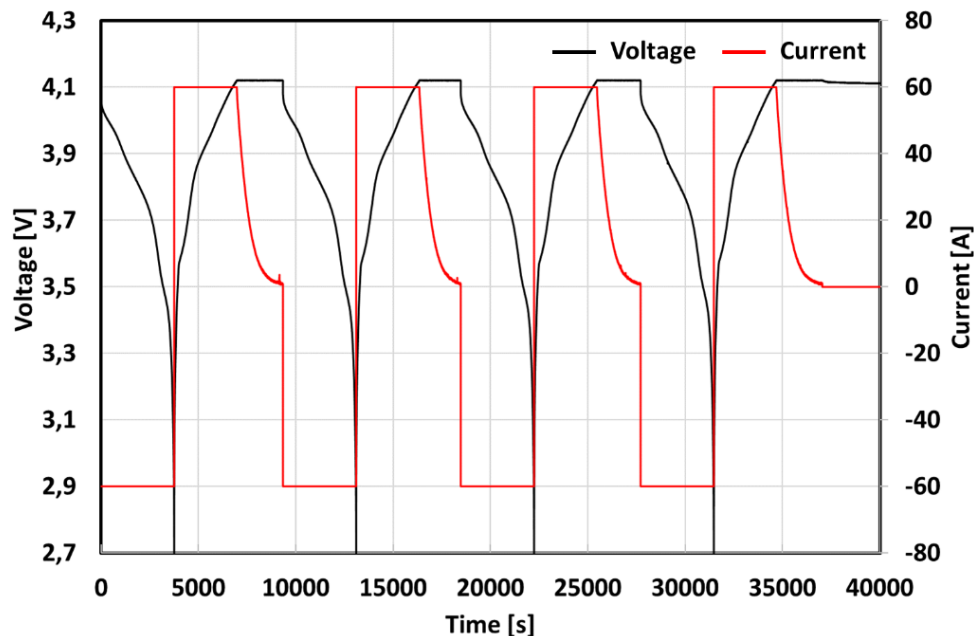

Figure 18: Capacity test performed with a prismatic lithium-ion battery cell at 1C (C-rate) charge (CC) and 1C discharge (CC-CV).
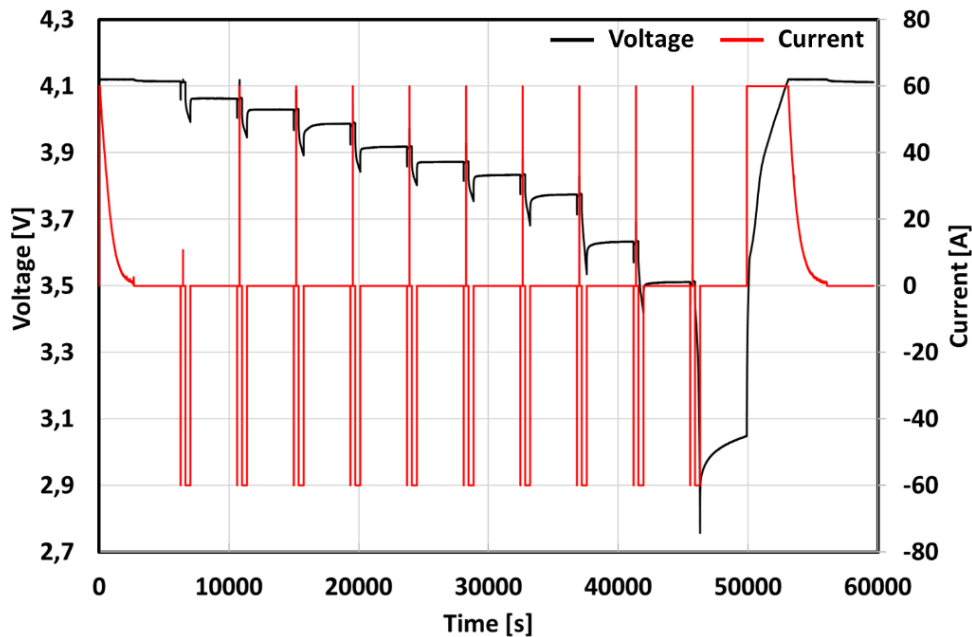
Figure 19: Pulse test performed with a prismatic lithium-ion battery cell with 10s pulse at 1C charge (CC) and 1C discharge (CC-CV) and 3 minutes rest phase.

Table 12: Capacity test procedure

Step	Description	Parameter	Stop Condition
1	Temperature conditioning	T = 25 °C	t = 1 h
2	CC Discharge	I = 63 A	V = 2,7 V
3	CC-CV Full Charge	I=63 A CV = 4,2V	I = 0,2A
4	CC Discharge	I = 63 A	V = 2,7 V
5	Repeat from 3 to 4		Counter = 3
6	CC-CV Full Charge	I=63 A CV = 4,2V	I = 0,2A

As described in Table 13, the pulse test encompasses a 10s discharge at 1C (63A), a 3-minute wait phase, a 10s charge at 1C, a 3-minute wait phase. A 1C discharge of 10% of the capacity is then performed. It is assumed to be 10% of SOC. Finally, a 1-hour rest is accomplished. The procedure is repeated until the lower cut-off voltage is reached.

Table 13: Pulse test procedure

Step	Description	Parameter	Stop Condition
1	Temperature conditioning	T = 25 °C	t = 1 h
2	CC-CV Full Charge	I=63 A CV = 4,2V	I = 0,2A
3	Rest		t = 1 h
4	CC Discharge	I = 63 A	t = 10s V = 2,7V
5	Rest		t = 3 min
6	CC Charge	I = 63 A	t = 10s V = 4,12V
7	Rest		t = 3 min
8	CC Discharge	I = 63 A	Discharge Capacity = 10% Capacity test V = 2,7 V
9	Rest		t = 1 h
10	Repeat from 4 to 9		Counter = 10
11	Rest		t = 1 h
12	CC-CV Full Charge	I=63 A CV = 4,2V	I = 0,2A

5.3. Test facilities

The experimental tests were performed in the laboratories of CNR ITAE in Messina. The instrumentation used for the electrical characterization includes a Bitrode cell cycler, able to manage up to 2 channels in parallel with a maximum of 500A in a 0-20V voltage range and an Angelantoni climatic chamber model 600L. The characteristics of the instrumentation used are shown in the following Table 14.

Table 14: Test facilities

BATTERY CYCLERS	
Bitrode FTV-1 Number of Circuits: 2 Max output power: 20 kW Voltage range: 0 - 20 V Voltage Resolution: 0.001 V Max Current per circuit: 500 A (up to 1000 A in parallel) Current Ranges: 500 A; 100 A; 10 A Current Resolutions: 0.1 A; 0.01 A; 0.001 A Channel inputs: Type J Thermocouples Range: -40 to 200 °C Resolution: 0.5 °C Acquisition rate: 0.1 s *Electrical Characterization: cycling with customized profiles both automotive and stationary* *Abuse test: over charge, over discharge, short circuit, stress tests* *Endurance tests*	

CLIMATIC CHAMBERS

Angelantoni Discovery DY600

Safety degree EUCAR 6

Temperature range: -40 °C - +180 °C

Humidity range: 10% - 98% (+5 °C - +95 °C)

Internal dimensions: 850x740x890 mm (600 l)

Thermo-climatic tests: reproducing particular ambient conditions for tests like damp heat, dry heat, sub-zero, thermal cycles

Cold Cranking tests

Endurance tests

Current and voltage measurements of the electrochemical cell were performed using the cyclator's internal electrical characterization module. The T-type copper/constantan thermocouple associated with the power channel of the cycler were used to detect the thermal behavior of the cell. The system is capable of detecting and recording:

- Charge and discharge current [A];
- Voltage at module terminals [V];
- Capacity charged and discharged [Ah];
- Power charged and discharged [Ah];
- Temperature [°C].

The internal temperature of the climatic chamber, containing the cell under test, was monitored using Pt100 resistance thermometer. The measurement of relative humidity is based on a psychrometric system (dry bulb, wet bulb) in which the control system detect the temperature value of dry and wet bulb and calculates the relative humidity.

5.4. Test schedule

The ageing test campaign using the WLTP CLASS 3B cycle was carried out following a procedure, which involved the sequence of tests shown in Table 15.

Table 15: Ageing test with WLTP CLASS 3B driving cycle

Step	Parametric checks	Driving cycles	Total driving cycle	Total ageing test years
1	Capacity + Pulse test	261	261	½ year
2	Capacity + Pulse test	262	523	1 year
3	Capacity + Pulse test	261	784	1 ½ year
4	Capacity + Pulse test	262	1046	2 year
5	Capacity + Pulse test	261	1307	2 ½ year
6	Capacity + Pulse test	262	1569	3 year
7	Capacity + Pulse test	261	1830	3 ½ year
8	Capacity + Pulse test	262	2092	4 year
9	Capacity + Pulse test	261	2353	4 ½ year
10	Capacity + Pulse test	262	2615	5 year
11	Capacity + Pulse test	261	2876	5 ½ year
12	Capacity + Pulse test	262	3138	6 year
13	Capacity + Pulse test	261	3399	6 ½ year
14	Capacity + Pulse test	262	3661	7 year
15	Capacity + Pulse test	261	3922	7 ½ year
16	Capacity + Pulse test	262	4184	8 year

6. Results and Discussion

6.1. Cells inspection and Beginning of Life (BOL) conditions

At the beginning of the work, different cells are taken into account for ageing test. The first step before starting the ageing tests is to visually inspect the cells to make sure they are not damaged. Capacity tests are then conducted to evaluate the cells capacity. The cell with parameters close to those given in the manufacturer's datasheet was chosen for ageing tests (Table 16).

Table 16: Main parameters of cells at the BOL

	Ageing tests	Discharge Capacity (Ah)	Discharge Energy (Wh)	Energy Efficiency (%)
Cell 1	Driving cycle 25°C	64,26	241,03	96,01

6.2. Cells cycling under current driving cycle

The current driving cycle was applied to Cell 1. During each step of the ageing test the cell starts from the fully charged condition (SOC = 100%). Upon reaching the voltage of 3,1V, identified as the minimum safety voltage, the charging phase is triggered. Under these conditions the full discharge of the Cell 1 is about 6 current driving cycles. However, current driving cycles will age the Cell 1 over time causing a degradation leading to a shorted time to reach the lower cut off voltage than under BOL conditions. For the recharging phase, it is known that electric vehicles require rather long charging times. However, electric vehicles can be recharged faster by using high power charging stations (e.g., DC fast stations) [43]. Therefore, a charging time below one hour has been assumed only with a CC charging until the upper cut off limit without a CV charging phase. In Figure 20 a single step of ageing test with WLTP CLASS 3B driving cycle is reported. The value of SOC was computed by considering the capacity discharged from Cell 1 during the tests.
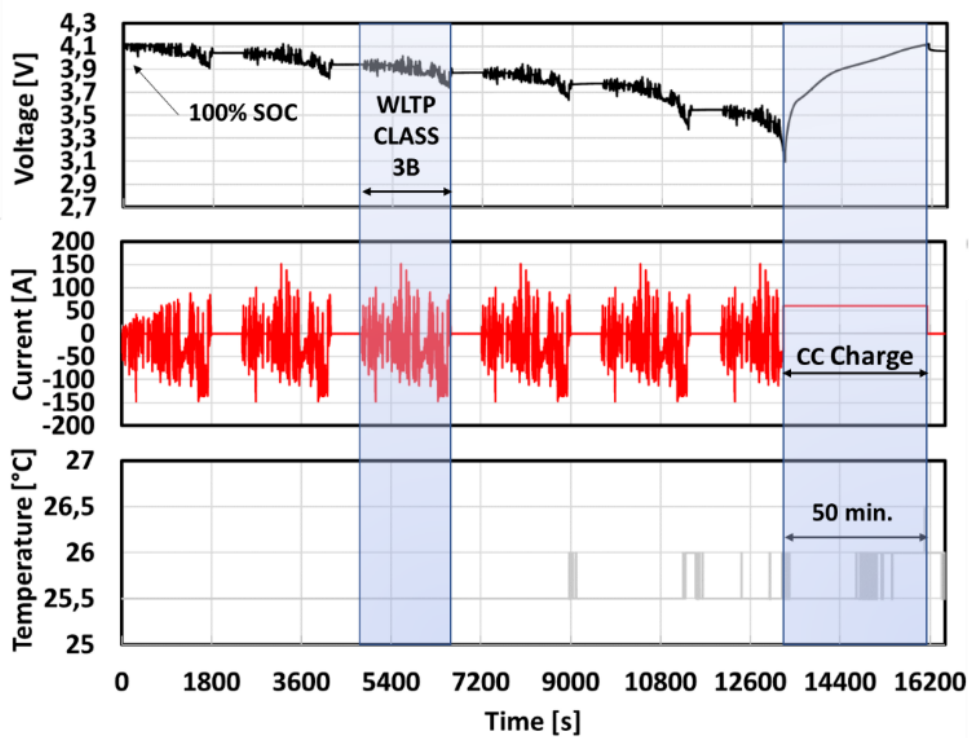
Figure 20: Voltage current and temperature profiles recorder during a single step of ageing test of driving cycle ageing at 25°C

Figure 21 shows the evolution of both charge and discharge voltage profiles as a function of the capacity, along different equivalent years of driving cycle ageing. Voltage profiles have been recorded during the parametric check-up tests at 1C. A reduction in available cell capacity of 11% and alterations in the shape of the curves after a series of test equivalent to 8 years was found.

a)

b)
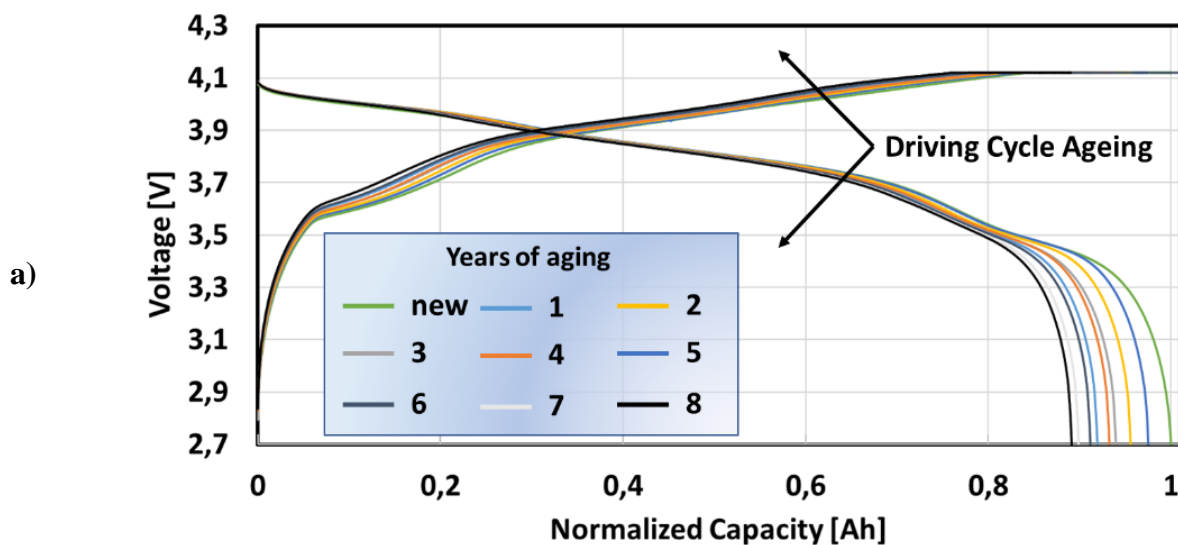
Figure 21: (a) Charge and Discharge time diagram during WLTP CLASS 3B driving cycle at 25°C from BOL to 8 test years of ageing (b) Capacity drop after battery ageing
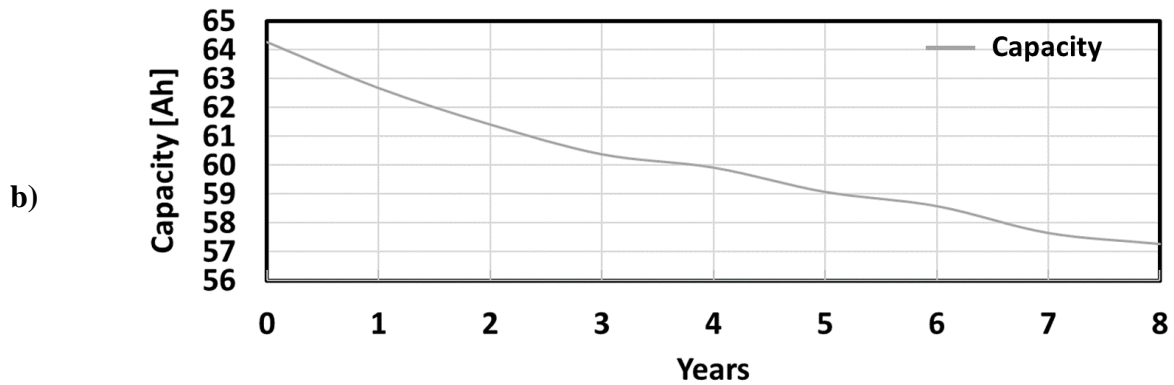
Pulse tests were accomplished to identify the internal resistance of Cell 1 during various stages of ageing at different SOC. The resistance of the battery was computed as voltage to current ratio. Several phenomena contribute to the voltage drop, they can be identified with a contribution due to all electronic resistances, the battery's electrolyte resistance, the battery's double layer capacitance and charge transfer resistance, and the polarization resistance which accounts for ionic diffusion in the solid phase [44]. The cell internal resistance (IR) depend on the interval Δt at which voltage and current samples are taken and also depend on SOC battery. Resistance values at various SOC levels in 10% steps were extracted from the pulse tests. The applied driving cycle did not cause a large increase in the internal resistance of the cell under test. This value is confirmed by the energy efficiency value of the cell remaining almost constant. Probably during the first ageing the cell conditioned itself by improving performance and then remained stable as shown in Figure 22.
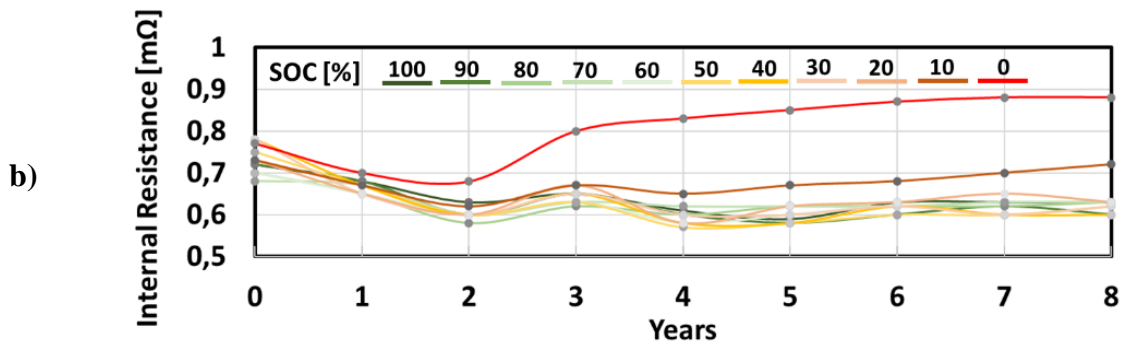
a)

b)
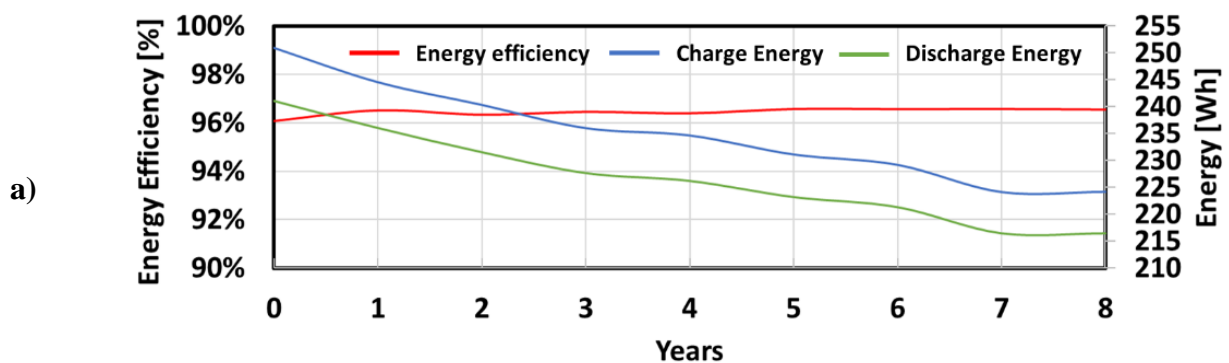
Figure 22: a) Evolution of Charge and Discharge Energy and Energy efficiency with ageing. b) Evolution of Internal cell resistance for different SOC values with ageing.

To further investigate the cell behaviour during lifetime IC and DV analysis were also performed. These analyses are two techniques widely applied to identify and quantify degradation mechanism in lithium-ion batteries [45]. The plateaus in charge and discharge voltage profiles represent phase transitions occurring due to electrochemical reactions, which can be highlighted after differentiation of the curve, by the presence of well defined peaks. IC analysis, performed differentiating the capacity with respect to the voltage, allow to obtain peaks corresponding with the plateaus of the voltage-capacity curve, while DV analysis differentiates the terminal voltage with respect to cell capacity and shows peaks corresponding to the valleys of IC curve. By the analysis of both techniques, feature of interests (FOI) can be identified on the differential curves. The most relevant FOIs of IC curve include intensity, position, and the area under the peaks, while for DV curve the distance between the two adjacent peaks is the main FOI. In particular, the degradation mechanisms can be related to IC peak shifts toward lower voltage are associated with IR, the decrease of IC peaks intensity linked to LAM, and DV peaks shift coupled with both LAM and LLI [46].

In Figure 23 is shown the evolution of the IC curve obtained by differentiating the 1C discharge curves at different levels of ageing (years). It should be noted that, here a high C-rate was used to acquire voltage capacity curve, even though IC and DV often require a signal very close to the equilibrium condition of the cell. Despite the voltage curves used in the present work to perform differential analysis were acquired at 1C, the signals provided were still useful for identifying the most relevant signature typical for the chemistry of the cell under investigation. Indeed, as already proven in previous works, higher C-rate can be still useful for ageing mechanism identification [47][48]. By observing the IC curve three different peaks A, B and C can be identified at 3,47 V, 3,8 V and 4,1 V, respectively, which can be related to the graphite anode signatures [49]. On another

41

hand, the cathode phase transitions are not visible on the curve. Nevertheless, the overall shape of the curve suggests that the cathode chemistry is a combined LMO/NMC composition as already report for the same cell [39]. The most important variations as effect of the ageing are observed on peak A, which dropped almost 36% and shifting of 5 mV to higher potential in comparison to the fresh cell. Lower decreases of the intensity close to 10% are also observed for both peaks B and C. Despite the evolution in intensity, the positions of both peaks B and C on IC curves remains almost unchanged. On the basis of previous interpretations of the IC curve to identify the degradation mechanisms [50]-[51], the evolution of peak A can be mainly related to LLI, while the constant decrease of both peak B and C can be due to LAM of the negative electrode. As regard the peaks position, during discharging the change in voltage is negative and the peak in the IC graph are shifted to lower potentials because of the overvoltage caused by the polarization resistance [52]. Since the shift of peak A with ageing is in opposite direction and both peaks B and C remain unchanged, in agreement with the internal resistance evaluated by the pulse test, also IC analysis confirms that no relevant IR loss occurs. It is worth noting that, by proceeding with ageing a small peak at about 3,62 V appears, becoming well distinguished on IC curve matching with 8 years ageing. This peak, representing a typical signature of cathode material, may be masked due slow kinetic of the transformation and the high C-rate of the analysis, which does not allow to detect the process. On another hand, once the contribution from the negative electrode on the peak shape over cycling is eliminated, the effect of cathodic reaction is made evident on IC curve [53].
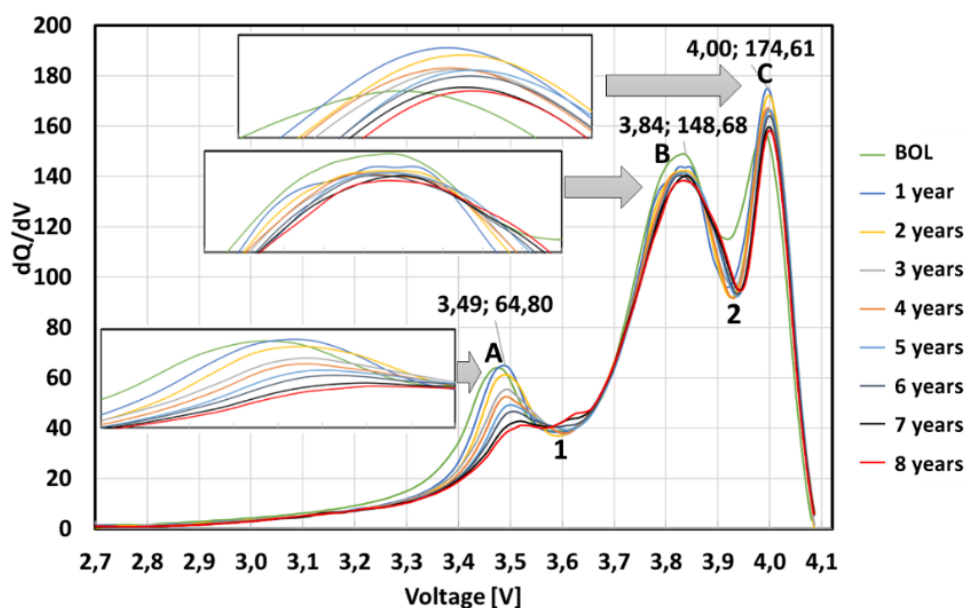

Figure 23: Evolution of IC profiles as effect of driving cycle ageing.

Figure 24 deals with the evolution of DV curve when differentiating the 1C discharge voltage profiles, similarly to what was done for IC analysis. The DV curve shows two peaks, which match with the valleys 1 and 2 in IC the curve and are representative of the anode signature of the cell. No cathode signatures are instead observable in DV curve as already reported for similar batteries when full cell voltage profile is used for the analysis [54]. In order to deeply investigate the degradation mechanisms of the cell, the peak 2, which indicates a 50% graphite lithiation, is used as reference process. It is to be noted that for the cell under investigation this peak is centred at about 75% of the total capacity, which suggest that the anode is overhang as typically for lithium battery [55]. This peak divides the DV spectra in two regions identified as distance Q1 and Q2 in Figure 25. The evolution of the distance Q1 with ageing can provide information about alteration on lithium storage capability of the graphite anode, then it is representative of anode degradation due to LAM. On another hand, Q2 gives information about cycling lithium between anode and cathode, therefore its change is indicative of possible LLI side reaction [56].

Figure 26 deals with the progression of both Q1 and Q2 parameters as effect of equivalent years of ageing under WLTP CLASS 3B driving cycles. Q1 change rapidly in the first year decreasing its value from 46,7 to 43,2 Ah then holding essentially the same value for the following cycles. On the contrary, a larger variation of the Q1 value can be observed, with a slight increase during the first year, and a progress drop proceeding with cycle ageing. The evolution of Q1 suggests that, after an initial loss of storage capability of the anode it is almost unchanged, then a slow degradation occurs with the cycles in following years. This observed behaviour suggests that during the first driving cycles the anode undergoes an initial conditioning due to the repeated volume changes of the graphite grains during lithiation and delitiation phases. As well known, these contraction and expansion lead to the formation of particle cracking or to the detachment of the active material from the electrode with consequent isolation of the particles and therefore to loss of active material (LAM) [57]. The lack of further evolution of Q1 after the first few cycles could mean that, following the initial rearrangement of the anode material, there is no longer a relevant LAM of the negative electrode. In contrast, Q2 follows a linear loss of capacity, suggesting that LLI is the dominant degradation mechanism induced by WLTP CLASS 3B driving cycles on the DUT. This ageing mechanism is in agreement with previous literature for the chemistry of the DUT and it is attributed to the continuously slow growth of the SEI layer on the negative graphite electrode [58]-[60]. However, a more detailed analysis of the trend of Q2 during the first year shows a slight increase in capacity compared to the fresh cell, which could be related to a larger amount of cycling lithium inside the cell. To better

understand this phenomenon, it is possible to analyse the change in the shape and height of the peaks in the DV curve. Regarding peak 2, corresponding to the phase transformation of the high SOC anode, it rises in intensity also becoming sharper during the first cycles corresponding to about the first year of ageing, then shifts to the right keeping the shape and magnitude unchanged. The magnitude of the peaks is usually related to the degree of homogeneity of lithium distribution (HLD) inside the cell, and in particular, the increase in intensity due to the charge and discharge cycles could be explained by an improvement in the HLD compared to the fresh cell not yet adequately conditioned [61]-[62]. A result similar to the one just discussed was obtained by Sieg et al. [63] investigating the ageing phenomena induced by an EV driving profile on a cell based on NMC cathode. They observe that the peak shown in the differential voltage curve at high SOCs corresponding to an anode transformation shows an increase during the first few cycles and then decreasing over time due to the effect of cycles on the cell. Such an evolution of peak intensity has been related to an initial enhancement of the HLD of the cell and then to a change in graphite material or microstructure. Further confirmation of the improvement in HLD comes from the analysis of peak 1 in Figure 24. As ageing progresses, a shoulder appears on the right side of peak 1. The reason for this phenomenon has been related to the enhancement of HLD as an effect of fresh cell cycling [64]. Although this phenomenon typically occurs immediately after the first full charge cycles [65], we observed it only after having carried out several driving cycles. Since this homogenization of lithium occurs when the slope in the voltage curves of one electrode is remarkably high compared to the counterpart electrode, it is plausible that since the driving cycle operates mainly within intermediates SOC, rarely reaching the end of charge or discharge delaying the phenomenon over time.
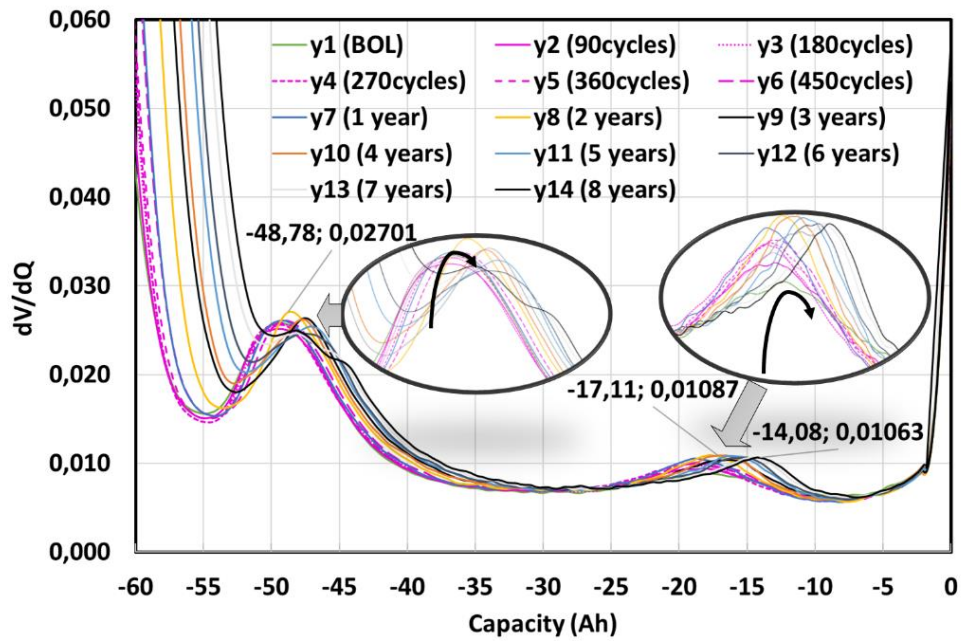
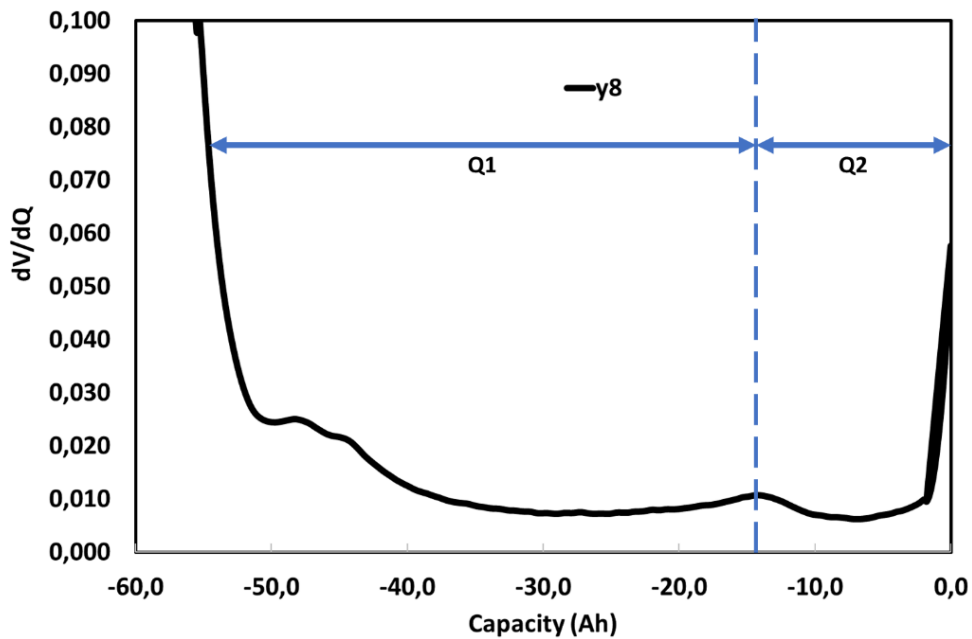Figure 24 Evolution of DV profiles as effect of driving cycle ageing

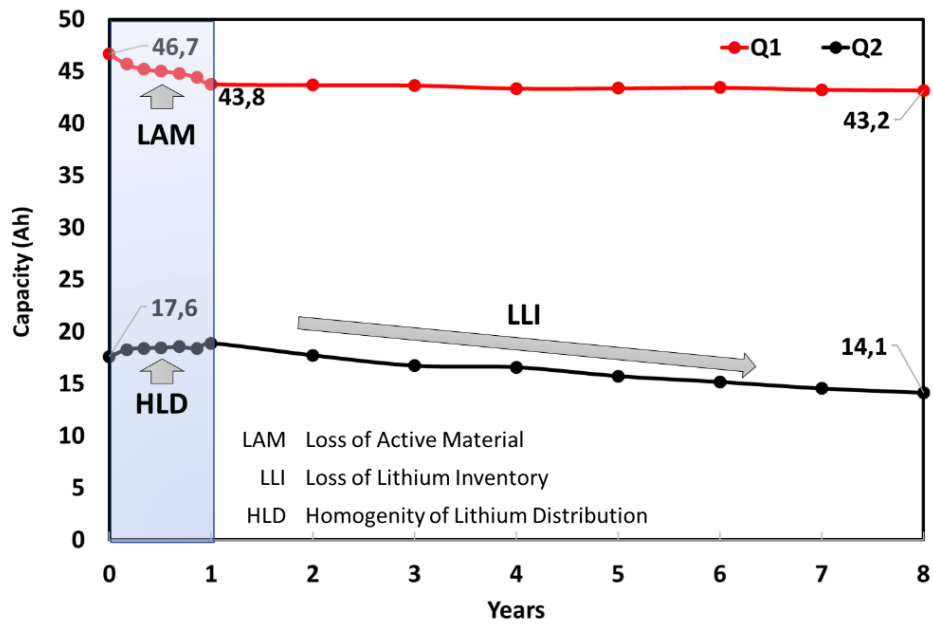Figure 25: Identification of the Q1 and Q2 regions in DV spectra indicative of LAM and LLI, respectively

Figure 26: Evolution of Q1 and Q2 regions during the driving cycle ageing and ageing mechanisms.

6.3. Lifetime modeling

In order to estimate the overall capacity loss of an electrochemical commercial graphite/LMO-NMC lithium-ion cell, it is necessary to estimate the capacity loss related both to driving cycle and calendar ageing. A mathematical representation of the capacity loss resulting from the two contributions is given in the equation (1):

$$C_r = C_{BOL} - C_{driving\_loss} - C_{calendar\_loss} \tag{1}$$

Where C_r is the residual capacity of the cell at time t, C_{BOL} is the initial capacity of the cell under test at the beginning of its life, $C_{driving\_loss}$ is the capacity loss when it is working due to the driving cycle, and $C_{calendar\_loss}$ is the capacity loss related to the time in which the cell is not working. $C_{driving\_loss}$ represents the capacity loss due to driving cycle ageing expressed in percentage.

$$C_{driving\_loss} = 100 - 0,0875 \cdot t^{0,6} \tag{2}$$
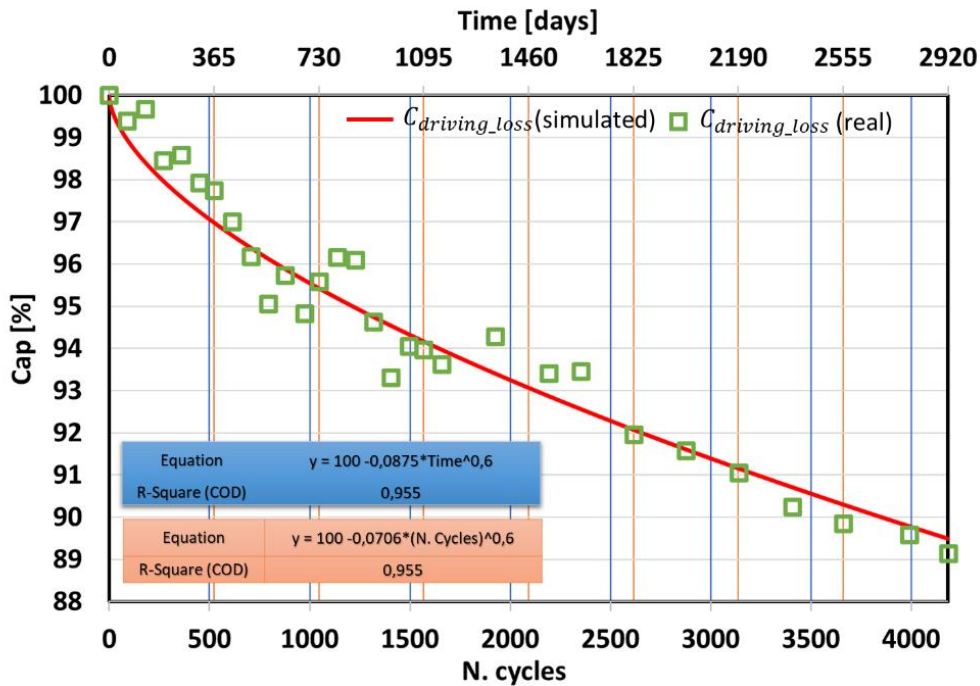

Figure 27: Loss of capacity from number of driving cycle WLTP CLASS 3B and days.

In order to evaluate the effect of calendar ageing, some curves were extracted from [27] for a cell with the same characteristics of the DUT. In our case it was found that an equation similar to that of the driving cycle ageing fitted very well the calendar ageing curves and it is described in (3).

$C_{calendar\_loss}$ represents the capacity loss due to calendar ageing expressend in percentage value, a is the initial capacity of electrochemical cell, b is a parameter that depends on the temperature and SOC, t is the time period while the power coefficient c is a constant as reported in Table 17. The coefficient of determination (R square) of the fitting performed is also given in Table 17 for the ageing curves considered. Under these conditions, the only temperature and SOC-dependent parameter that can describe the evolution of the cell capacity fading related to calendar ageing is b. The following figures (Figure 28 and Figure 29) deal with experimental data of capacity loss as effect of calendar ageing for the available combination mentioned above. Moreover, the dotted lines represent the fitting curves according to equation (1) with the parameters of Table 17. As shown in Figure 28 and Figure 29 the decay is higher when the battery is in stand by at high SOC.

$$C_{calendar\_loss} = a + b \cdot t^c \qquad\qquad (3)$$

Table 17: R-square fitting curve (3)

Temperature [°C]	SOC [%]	a	b	c	R²
0	0/30/45/80/100	100	-0,0899	0,6	0,9692
25	80	100	-0,1796	0,6	0,9987
45	0	100	-0,0446	0,6	0,8357
45	30	100	-0,3097	0,6	0,9829
45	65	100	-0,5609	0,6	0,9487
45	80	100	-0,5277	0,6	0,9790
45	100	100	-0,5380	0,6	0,9941
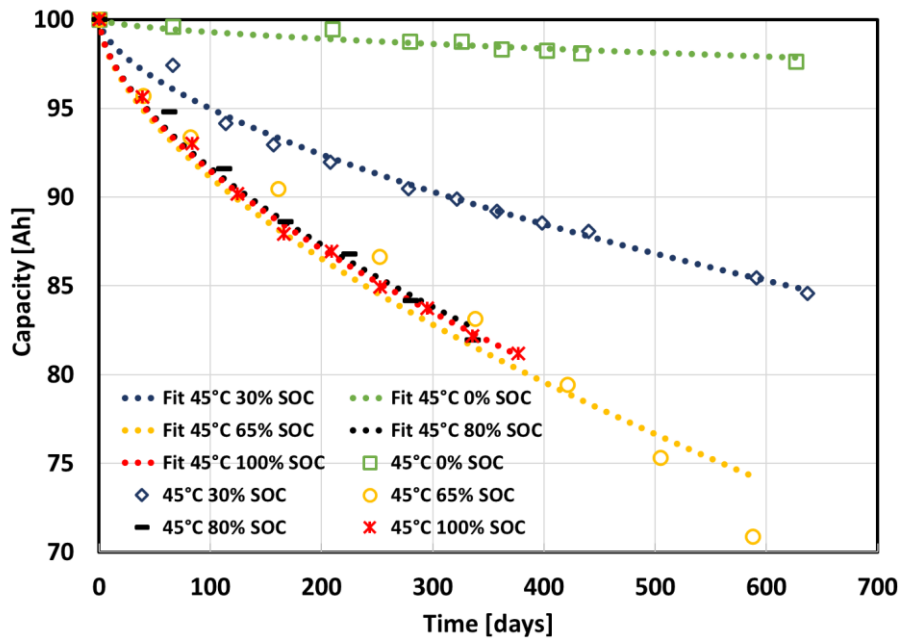
Figure 28: Calendar ageing data and curve fitting at 45°C and different SOC levels [27].
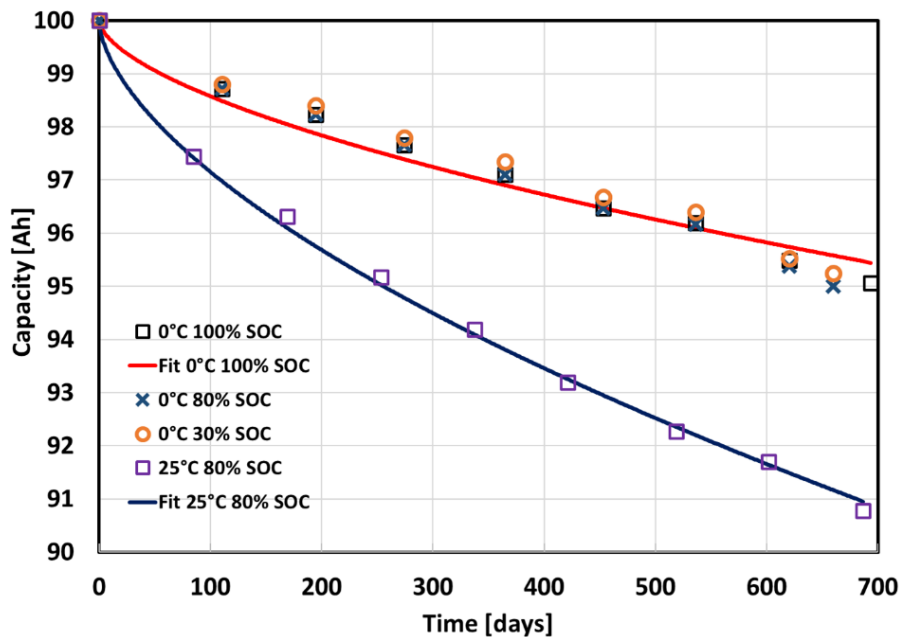
Figure 29: Calendar ageing data and curve fitting at 0°C and different SOC levels and 25°C and 80% SOC levels [27].

The fitting carried out on experimental data allowed parameter b to be computed only for the available combinations of SOC and Temperature. Since only experimental data of eleven storage conditions were available, it was therefore necessary to estimate this parameter for different values of SOC and

Temperature within the range of interest. The variation of parameter b with respect to temperature and SOC is shown in Figure 30. In the surface, it can be seen that parameter b takes higher values as SOC and temperature increase indicating that the loss of capacity due to calendar ageing is amplified under these conditions.
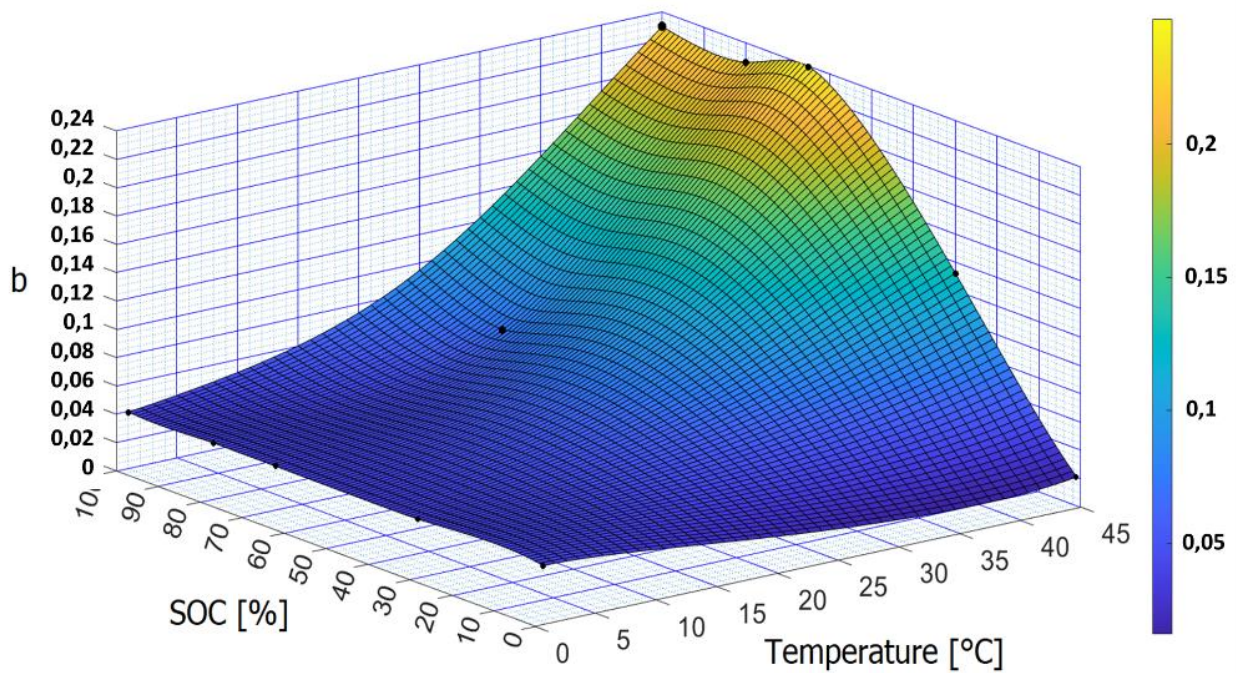
Figure 30: 3d variation of b parameters with SOC and Temperature.

The overall ageing of an electrochemical cell subjected to driving cycle and calendar ageing was then evaluated. The effects are considered to be separated in time because calendar ageing applies when the vehicle is parked and is not being used, unlike the driving cycle ageing. In order to identify a real vehicle usage, average data on distance travelled in Europe were used [38] with an average distance travelled on a weekday of 32,8 km and an average distance travelled on a public holiday of 34,6 km. Assuming a typical year consisting of 365 days including 261 weekdays and 52 weekends (104 days), the total distance is 12.168,12 km. It was then assumed that the WLTP_CLASS_3B driving cycle was used as the standard route as reported in Table 18.

Table 18: Typical yearly vehicle utilization according to distance travelled in Europe

	Weekdays	driving cycles	Weekdays	driving cycles
WLTP CL. 3B	*154*	*1*	*53*	*1*
(*23,266 km*)	*107*	*2*	*51*	*2*
Yearly distance	*8.562 km*		*3.606 km*	

An average daily temperature for the 8 years of test was considered to make this calculation, in particular, referring to a real situation in Messina, Italy [66]. Similarly, considering the effect of range anxiety involving a driver of an electric vehicle, it was assumed that the driver would never want to find himself with a residual range of less than 30% [67][68]. To better define the range anxiety, it is the fear of not being able to find an electric recharging station before the battery runs out. Therefore, the SOC value variation due to driving cycle is between 30% and 100% and depends on the previous SOC value of the cell reached after the last driving cycle done and computed from the vehicle model described above. Instead, the calendar ageing was computed for each partial day (excluding the time required to perform the driving cycle and the recharging phase if required) and it is affected of reached SOC and temperature. A typical year variation of Temperature, initial daily SOC and number of driving cycles are depicted in Figure 31.
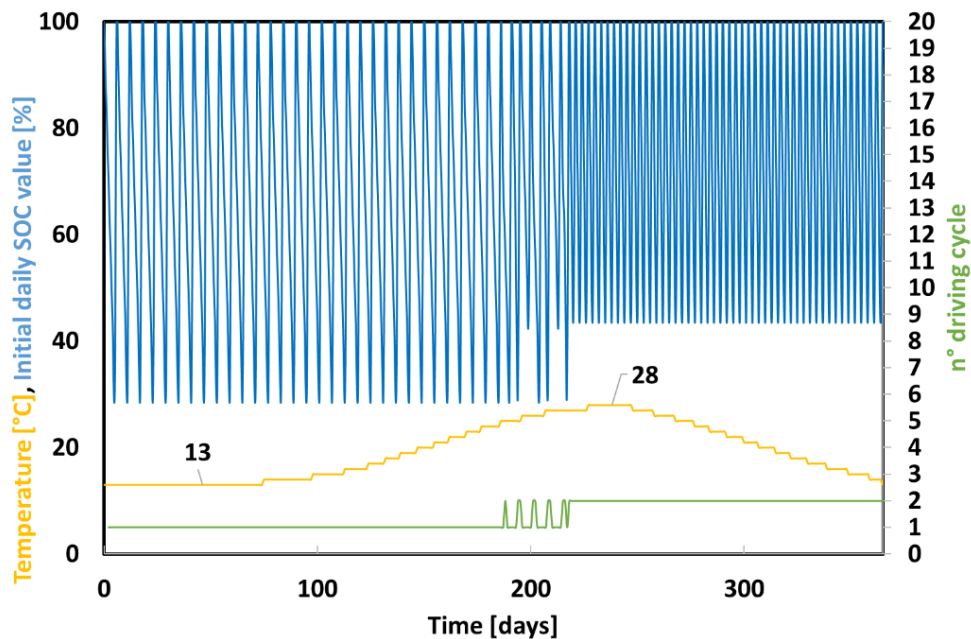

Figure 31: Temperature, initial daily SOC value and number of driving cycle in a year.

A time period of 8 years was considered to evaluate the capacity loss for calendar and driving cycle. A cell charging is done when the voltage is below 3,1V assessed as a SOC lower than 30%. After the charging period, the upper voltage cut off of the cell is 4,12V (100% SOC). The number of daily WLTP driving cycles were distributed as shown in Table 18. The total capacity loss was then computed for an 8-year time frame and the annual percentages is shown in Table 19.

Table 19: Typical yearly vehicle utilization

year	$C_{calendar\_loss}$	$C_{driving\_loss}$	$C_{remaining}$
0	0	0	100,00
1	5,03	3,02	91,95
2	2,76	1,56	87,63
3	2,25	1,26	84,12
4	1,97	1,10	81,06
5	1,78	0,99	78,29
6	1,64	0,92	75,73
7	1,54	0,86	73,34
8	1,45	0,81	71,08

A number of possible scenarios were then evaluated in order to predict the capacity loss as shown in Table 20. Scenarios 1 and 2 describe a situation in which both the environment temperature and the battery pack conditioning system hold the battery operating temperature at 15°C (Scenario 1) or 35°C (Scenario 2). The other scenarios simulate more intensive uses of the vehicle, for example with commercial vehicles. Scenario 3 describes a daily vehicle driving use of 1 hour, Scenario 4 describes a daily vehicle driving use of 2 hours, Scenario 5 describes an intensive daily vehicle driving use of 6 hours. The last three scenarios are repeated from scenarios 3, 4 and 5 with the difference that the ambient temperature is 35°C. For each Scenario the WLTP CLASS 3B driving cycle is used as reference. The scenarios were defined considering that the working temperature of a battery pack during the driving cycle ranges from 15 to 35 °C. From data computed at 25°C for the driving cycle, the temperature related ageing factor is reported in [42]. To evaluate the scenarios, the number of actual driving cycles were related to the number of daily driving cycles required for the scenarios limiting to 4184 the number of actual driving cycles performed. According to these considerations, a calendar capacity loss was computed as the difference between the daily time (24 hours) and the time

needed to perform driving cycles. Figure 27 deals with the loss of capacity for each step of driving cycles considered and the fitting curve.

Table 20: Annual vehicle use scenarios

Scenario	Battery working temperature [°C]	Ambient Temperature [°C]	Yearly distance [km]
1	15	15	12.168
2	35	35	12.168
3	15	15	16.984,18
4	15	15	50.952,54
5	15	15	101.905,08
6	35	35	16.984,18
7	35	35	50.952,54
8	35	35	101.905,08

Estimating the residual capacity of an EV battery at the end of its operational life is another important aspect for possible further uses, because it still has usable residual capacity. Refurbished EV batteries can be and advantageous alternative to brand new batteries in less stressful applications such as stationary applications. The results obtained can also be used to estimate the maximum range of a vehicle with a second life battery. The analysis presented through the proposed scenarios is an example of possible use, and the data obtained are shown in Table 21 and Table 22. Herein a reported the remaining capacity of the battery pack for the different Scenario along the years. Moreover, the overall C reached within the thirty percent of capacity loss and the single contributes of calendar and capacity loss.

Table 21: Estimated capacity loss percentage in the vehicle according to the scenarios @ 15°C

Years	Scenario 1	Scenario 3	Scenario 4	Scenario 5
0	100,00	100,00	100,00	100,00
1	93,78	93,53	91,51	89,40
2	90,58	90,18	87,13	83,93
3	87,99	87,47	83,59	79,50
4	85,73	85,11	80,50	75,64
5	83,69	82,98	77,71	72,15
6	81,80	81,01	75,13	68,93
7	80,04	79,17	72,72	65,92
8	78,38	77,43	70,45	63,08
9	76,80	75,78		
10	75,28	74,19		
11	73,83	72,68		
12	72,43	71,21		
13	71,07	69,79		
14	69,76			
Overall km at 30% capacity loss	167.189	218.328	417.392	576.810
$C_{calendar\_loss}$ [%]	20,23	18,56	13,13	9,51
$C_{driving\_loss}$ [%]	9,77	11,44	16,87	20,49

Table 22: Estimated capacity loss percentage in the vehicle according to the scenarios @ 35°C.

Years	Scenario 2	Scenario 6	Scenario 7	Scenario 8
0	100,00	100,00	100,00	100,00
1	84,45	84,16	80,08	75,13
2	76,48	75,99	69,79	62,30
3	70,04	69,38	61,47	51,92
4	64,42	63,60	54,21	
5	59,34	58,39		
6	54,66	53,58		
7	50,28			
Overall km at 30% capacity loss	36.550	49.230	100.788	139.316
$C_{calendar\_loss}$ [%]	21,28	19,59	14	10,56
$C_{driving\_loss}$ [%]	8,72	10,41	16	19,44

In order to compare the effect of the different Scenario was assumed a 30 percent of capacity loss as limit to define the useful life of the battery. In Table 21 is shown the remaining capacity under different scenario at the fixed temperature of 15°C and for different yearly distance. Comparing the different scenarios, a 30% of loss of capacity is reached after about 13 years for the best Scenario (Scenario 1 -12.168km/year). While in the worst case (Scenario 5 – 101.905 km/year) the same loss of capacity is reached after only 5 years with a consequence reduction in vehicle life of about 8 years. Similarly in Table 22 are reported the same yearly distance as in Table 21 but at fixed temperature of 35°C. The proposed scenarios show a strong impact of temperature on the ageing of the electrochemical cell, which decreases from 14 years to about 3 years in the best case in terms of kilometres travelled (Scenario 1 vs Scenario 2). In the worst case in terms of kilometres (Scenario 5 vs Scenario 8), the temperature impact decreases the lifetime of the battery pack from 5 years to about 1 year. In conclusion a data comparison of all Scenarios highlights a strong impact of temperature on both calendar and cycling ageing capacity loss. It is worth noting that in case of less intensive scenarios, calendar ageing is the most relevant contribute on the overall capacity loss because the battery spends most of the time in resting condition. On the other hand, in the case of more intensive scenarios in terms of yearly distance, the battery spends more time in driving conditions with the consequence that cycle ageing contributes more than calendar ageing.

7. Conclusions

The capacity loss over the time is an aspect of paramount importance for LI-ion batteries for EV, as it affects the vehicle range and performance. In this Ph.D. thesis has presented a procedure to estimate the progressive reduction of the capacity in Li-ion batteries from datasheet information. Subsequently experimental ageing tests on a lithium-ion battery for electric vehicles with up to 10% capacity loss. Experimental tests are performed to investigate lithium-ion cell degradation under WLTP CLASS 3B driving cycle. The lithium-ion battery considered in this paper consists of a LMO-NMC cathode and a graphite anode with a capacity of 63Ah used in EV applications. A vehicle model was used to convert the WLTP CLASS 3B driving cycle into an electrochemical cell level scaled current profile. The cell under test was aged at room temperature (25°C) for a number of cycles equal to 8 test years (4184 cycles) excluding calendar ageing. IC and DV analysis were also performed to understand the evolution of the ageing process. The main outcomes are summarized below:

- A suitable procedure has been developed to assess the reliability of a lithium-ion battery for EV taking into account operating conditions.

- A reduction in available cell capacity of 11% after 8 test years from BOL condition is found and it does not cause a large increase in the internal resistance.

- IC curve shows three different peaks mainly related to LLI and LAM of the negative electrode. Important variations are observed on the first peak, which dropped almost 36% and shifting of 5 mV to higher potential in comparison to the fresh cell after ageing.

- DV analysis shows an alteration on lithium storage capability of the graphite anode, then it is representative of anode degradation due to LAM. Q2 changing is indicative of possible LLI side reaction. An increment of peaks is noted in the first year. This evolution of peak magnitude has been related to an initial enhancement of the HLD of the cell and then to a change in graphite material or microstructure.

- From real data coming from WLTP CLASS 3B driving cycle a mathematical model for capacitance loss from cycle ageing was extracted.

- Real data retrieved from a literature article [27] were analysed and a mathematical curve dependent on temperature and SOC was extracted to estimate the calendar ageing.

- Total ageing was computed as the sum of calendar and driving cycle contributions for 8 years and different Scenarios were then evaluated in order to predict the capacity loss.

8. References

[1]   European Parliament. New EU regulatory framework for batteries Setting sustainability requirements.   10-03-2022. https://www.europarl.europa.eu/RegData/etudes/BRIE/2021/689337/EPRS_BRI(2021)689337_EN.pdf

[2]   Neil Hume, Emiko Terazono and Tom Wilson, European gas prices soar and oil tops $105 after Russia attacks Ukraine, Financial Times, https://www.ft.com/content/c6303127-5edf-4256-9c25-effa75766002

[3]   Reddy TB. Linden's Handbook of Batteries, Fourth Edition. 4th ed. New York: McGraw-Hill Educatio

[4]   Liu W, Placke T, Chau KT. Overview of batteries and battery management for electric vehicles. Energy Reports. 2022;8:4058-4084. doi:https://doi.org/10.1016/j.egyr.2022.03.016

[5]   Duh Y-S, Sun Y, Lin X, et al. Characterization on thermal runaway of commercial 18650 lithium-ion batteries used in electric vehicles: A review. J Energy Storage. 2021;41:102888. doi:https://doi.org/10.1016/j.est.2021.102888

[6]   Duh Y-S, Theng J-H, Chen C-C, Kao C-S. Comparative study on thermal runaway of commercial 14500, 18650 and 26650 LiFePO4 batteries used in electric vehicles. J En-ergy Storage. 2020;31:101580. doi:https://doi.org/10.1016/j.est.2020.101580

[7]   Verma A, Rakshit D. Performance analysis of PCM-fin combination for heat abatement of Lithium-ion battery pack in electric vehicles at high ambient temperature. Therm Sci Eng Prog. 2022;32:101314. doi:https://doi.org/10.1016/j.tsep.2022.101314

[8]   Eboli L, Mazzulla G, Pungillo G. How drivers' characteristics can affect driving style. Transp Res Procedia. 2017;27:945-952. doi:https://doi.org/10.1016/j.trpro.2017.12.024

[9]   Vetter et al., "Ageing mechanisms in lithium-ion batteries," J. Power Sources, vol. 147, no. 1, pp. 269–281, 2005

[10]   Wang A, Kadam S, Li H, Shi S, Qi Y. Review on modeling of the anode solid electrolyte interphase (SEI) for lithium-ion bat-teries. npj Comput Mater. 2018;4(1):15. doi:10.1038/s41524-018-0064-0

[11]   Lin C, Tang A, Mu H, Wang W, Wang C. Aging Mechanisms of Electrode Materials in Lithium-Ion Batteries for Electric Ve-hicles. Omar N, ed. J Chem. 2015;2015:104673. doi:10.1155/2015/104673

[12] Zhou w, hao f, fang d. the effects of elastic stiffening on the evo-lution of the stress field within a spherical electrode particle of lithium-ion batteries. int j appl mech. 2013;05(04):1350040. doi:10.1142/s1758825113500403

[13] Christensen J, Newman J. A Mathematical Model of Stress Generation and Fracture in Lithium Manganese Oxide. J Electro-chem Soc. 2006;153(6):A1019. doi:10.1149/1.2185287

[14] Zhou W. Effects of external mechanical loading on stress generation during lithiation in Li-ion battery electrodes. Electrochim Acta. 2015;185:28-33. doi:https://doi.org/10.1016/j.electacta.2015.10.097

[15] Petzl, M.; Kasper, M.; Danzer, M.A. Lithium Plating in a Commercial Lithium-Ion Battery

[16] A Low-Temperature Aging Study. J. Power Sources 2014, 275, 799–807, doi:10.1016/j.jpowsour.2014.11.065. - Waldmann, T.; Hogg, B.I.; Wohlfahrt-Mehrens, M. Li plating as unwanted side reaction in commercial Li-ion cells

[17] A review. J. Power Sources 2018, 384, 107–124, doi:10.1016/j.jpowsour.2018.02.063

[18] Petzl, M.; Kasper, M.; Danzer, M.A. Lithium Plating in a Commercial Lithium-Ion Battery—A Low-Temperature Aging Study. J. Power Sources 2014, 275, 799–807, doi:10.1016/j.jpowsour.2014.11.065

[19] Wu, C.; Zhu, C.; Ge, Y.; Zhao, Y. A Review on Fault Mechanism and Diagnosis Approach for Li-Ion Batteries. J. Nanomater. 2015, 2015, 8, doi:10.1155/2015/631263

[20] Lewerenz, M.; Marongiu, A.;Warnecke, A.; Sauer, D.U. Differential voltage analysis as a tool for analyzing inhomogeneous aging: A case study for LiFePO4|Graphite cylindrical cells. J. Power Sources 2017, 368, 57–67, doi:10.1016/j.jpowsour.2017.09.059

[21] Vetter J, Novák P, Wagner MR, et al. Ageing mechanisms in lithium-ion batteries. J Power Sources. 2005;147(1):269-281. doi:https://doi.org/10.1016/j.jpowsour.2005.01.006

[22] Birkl CR, Roberts MR, McTurk E, Bruce PG, Howey DA. Degradation diagnostics for lithium ion cells. J Power Sources. 2017;341:373-386. doi:https://doi.org/10.1016/j.jpowsour.2016.12.011

[23] Barré A, Deguilhem B, Grolleau S, Gérard M, Suard F, Riu D. A review on lithium-ion battery ageing mechanisms and esti-mations for automotive applications. J Power Sources. 2013;241:680-689. doi:10.1016/J.JPOWSOUR.2013.05.040

[24] Gailani A, Mokidm R, El-Dalahmeh M, El-Dalahmeh M, Al-Greer M. Analysis of Lithium-ion Battery Cells Degradation Based on Different Manufacturers. In: 2020 55th International

Universities Power Engineering Conference (UPEC). ; 2020:1-6. doi:10.1109/UPEC49904.2020.9209759

[25]   Su L, Wu M, Li Z, Zhang J. Cycle life prediction of lithium-ion batteries based on data-driven methods. eTransportation. 2021;10:100137. doi:https://doi.org/10.1016/j.etran.2021.100137

[26]   Svens P, Smith AJ, Groot J, Lacey MJ, Lindbergh G, Lindström RW. Evaluating Performance and Cycle Life Improvements in the Latest Generations of Prismatic Lithium-Ion Batteries. IEEE Trans Transp Electrif. Published online 2022:1. doi:10.1109/TTE.2022.3158838

[27]   Montaru M, Fiette S, Koné J-L, Bultel Y. Calendar ageing model of Li-ion battery combining physics-based and empirical ap-proaches. J Energy Storage. 2022;51:104544. doi:https://doi.org/10.1016/j.est.2022.104544

[28]   Gandoman FH, Jaguemont J, Goutam S, et al. "Concept of reliability and safety assessment of lithium-ion batteries in electric vehicles: Basics, progress, and challenges". Appl Energy. 2019; 251:113-343

[29]   Testa A, De Caro S, Panarello S, et al. "Stress analysis and lifetime estimation on power MOSFETs for automotive ABS systems". In: 2008 IEEE Power Electronics Specialists Conference. 2008:1169-1175

[30]   Testa A, De Caro S, Russo S. A Reliability Model for Power MOSFETs Working in Avalanche Mode Based on an Experimental Temperature Distribution Analysis. IEEE Trans Power Electron. 2012;27(6):3093-3100

[31]   Mapelli FL. Modeling of Full Electric and Hybrid Electric Vehicles. In: Stevic DTE-Z, ed. IntechOpen; 2012:Ch. 7

[32]   Tremblay O, Dessaint L, Dekkiche A. A Generic Battery Model for the Dynamic Simulation of Hybrid Electric Vehicles. In: 2007 IEEE Vehicle Power and Propulsion Conference. ; 2007:284-289

[33]   Canals Casals L, Amante García B, González Benítez MM. Aging Model for Re-used Electric Vehicle Batteries in Second Life Stationary Applications BT

[34]   Casals LC, Amante García B, Canal C. Second life batteries lifespan: Rest of useful life and environmental analysis. J Environ Manage. 2019;232:354-363

[35]   Project Management and Engineering Research. In: Ayuso Muñoz JL, Yagüe Blanco JL, Capuz-Rizo SF, eds. Springer International Publishing; 2017:139-151

[36]   Belt J, Utgikar V, Bloom I. Calendar and PHEV cycle life aging of high-energy, lithium-ion cells containing blended spinel and layered-oxide cathodes. J Power Sources. 2011;196(23):10213-10221. doi:10.1016/J.JPOWSOUR.2011.08.067

[37]   Technical specifications. BMW i3 (120 Ah). https://www.press.bmwgroup.com/global/article/attachment/T0284828EN/415571

[38]   Ahern A (UCD), Weyman G (UCD), Redelbach M (DLR). Analysis of National Travel Statistics in Europe; 2013

[39]   Stroe D, Schaltz E. Lithium-Ion Battery State-of-Health Estimation Using the Incremental Capacity Analysis Technique. IEEE Trans Ind Appl. 2020;56(1):678-685. doi:10.1109/TIA.2019.2955396

[40]   S. Micari, S. Foti, A. Testa, S. De Caro, F. Sergi, L. Andaloro, D. Aloisio, G. Napoli "Ageing effects prediction on Lithium-Ion Batteries in second-life applications," 2020 International Symposium on Power Electronics, Electrical Drives, Automation and Motion (SPEEDAM), Sorrento, Italy, 2020, pp. 201-206

[41]   Orecchini F, Santiangeli A, Zuccari F. Real Drive Well-to-Wheel Energy Analysis of Conventional and Electrified Car Power-trains. Energies. 2020;13(18). doi:10.3390/en13184788

[42]   Micari S, Foti S, Testa A, et al. Reliability assessment and lifetime prediction of Li-ion batteries for electric vehicles. Electr Eng. 2022;104(1):165-177. doi:10.1007/s00202-021-01288-4

[43]   Hemavathi S, Shinisha A. A study on trends and developments in electric vehicle charging technologies. J Energy Storage. 2022;52:105013. doi:https://doi.org/10.1016/j.est.2022.105013

[44]   Barai A, Uddin K, Widanage WD, McGordon A, Jennings P. A study of the influence of measurement timescale on internal resistance characterisation methodologies for lithium-ion cells. Sci Rep. 2018;8(1):21. doi:10.1038/s41598-017-18424-5

[45]   Xie W, He R, Gao X, et al. Degradation identification of LiNi0.8Co0.1Mn0.1O2/graphite lithium-ion batteries under fast charging conditions. Electrochim Acta. 2021;392:138979. doi:https://doi.org/10.1016/j.electacta.2021.138979

[46]   Pastor-Fernández C, Yu TF, Widanage WD, Marco J. Critical review of non-invasive diagnosis techniques for quantification of degradation modes in lithium-ion batteries. Renew Sustain Energy Rev. 2019;109:138-159. doi:https://doi.org/10.1016/j.rser.2019.03.060

[47]   Li Y, Abdel-Monem M, Gopalakrishnan R, et al. A quick on-line state of health estimation method for Li-ion battery with in-cremental capacity curves processed by Gaussian filter. J Power Sources. 2018;373:40-53. doi:https://doi.org/10.1016/j.jpowsour.2017.10.092

[48]   Leonardi SG, Aloisio D, Brunaccini G, et al. Investigation on the ageing mechanism for a lithium-ion cell under accelerated tests: The case of primary frequency regulation service. J Energy Storage. 2021;41:102904. doi:https://doi.org/10.1016/j.est.2021.102904

[49]   Dubarry M, Truchot C, Cugnet M, et al. Evaluation of commercial lithium-ion cells based on composite positive electrode for plug-in hybrid electric vehicle applications. Part I: Initial characterizations. J Power Sources. 2011;196(23):10328-10335. doi:https://doi.org/10.1016/j.jpowsour.2011.08.077

[50]   Dubarry M, Truchot C, Liaw BY. Synthesize battery degradation modes via a diagnostic and prognostic model. J Power Sources. 2012;219:204-216. doi:https://doi.org/10.1016/j.jpowsour.2012.07.016

[51]   Pastor-Fernández C, Uddin K, Chouchelamane GH, Widanage WD, Marco J. A Comparison between Electrochemical Im-pedance Spectroscopy and Incremental Capacity-Differential Voltage as Li-ion Diagnostic Techniques to Identify and Quanti-fy the Effects of Degradation Modes within Battery Management Systems. J Power Sources. 2017;360:301-318. doi:https://doi.org/10.1016/j.jpowsour.2017.03.042

[52]   Krupp A, Ferg E, Schuldt F, Derendorf K, Agert C. Incremental Capacity Analysis as a State of Health Estimation Method for Lithium-Ion Battery Modules with Series-Connected Cells. Batteries. 2021;7(1). doi:10.3390/batteries7010002

[53]   Dubarry M, Truchot C, Liaw BY, et al. Evaluation of commercial lithium-ion cells based on composite positive electrode for plug-in hybrid electric vehicle applications. Part II. Degradation mechanism under 2 C cycle aging. J Power Sources. 2011;196(23):10336-10343. doi:10.1016/j.jpowsour.2011.08.078

[54]   Fath JP, Dragicevic D, Bittel L, et al. Quantification of aging mechanisms and inhomogeneity in cycled lithium-ion cells by dif-ferential voltage analysis. J Energy Storage. 2019;25:100813. doi:https://doi.org/10.1016/j.est.2019.100813

[55]   Gyenes B, Stevens DA, Chevrier VL, Dahn JR. Understanding Anomalous Behavior in Coulombic Efficiency Measurements on Li-Ion Batteries. J Electrochem Soc. 2014;162(3):A278--A283. doi:10.1149/2.0191503jes

[56]   Keil P, Schuster SF, Wilhelm J, et al. Calendar Aging of Lithium-Ion Batteries. J Electrochem Soc. 2016;163(9):A1872-A1880. doi:10.1149/2.0411609jes

[57]   O'Kane SEJ, Ai W, Madabattula G, et al. Lithium-ion battery degradation: how to model it. Phys Chem Chem Phys. 2022;24(13):7909-7922. doi:10.1039/D2CP00417H

[58]   Xu J, Deshpande RD, Pan J, Cheng Y-T, Battaglia VS. Electrode Side Reactions, Capacity Loss and Mechanical Degradation in Lithium-Ion Batteries. J Electrochem Soc. 2015;162(10):A2026-A2035. doi:10.1149/2.0291510jes

[59]   Stiaszny B, Ziegler JC, Krauß EE, Schmidt JP, Ivers-Tiffée E. Electrochemical characterization and post-mortem analysis of aged LiMn2O4–Li(Ni0.5Mn0.3Co0.2)O2/graphite lithium ion batteries. Part I: Cycle aging. J Power Sources. 2014;251:439-450. doi:https://doi.org/10.1016/j.jpowsour.2013.11.080

[60]   Smith AJ, Svens P, Varini M, Lindbergh G, Lindström RW. Expanded In Situ Aging Indicators for Lithium-Ion Batteries with a Blended NMC-LMO Electrode Cycled at Sub-Ambient Temperature. J Electrochem Soc. 2021;168(11):110530. doi:10.1149/1945-7111/ac2d1746

[61]   Lewerenz M, Sauer DU. Evaluation of cyclic aging tests of prismatic automotive LiNiMnCoO2-Graphite cells considering in-fluence of homogeneity and anode overhang. J Energy Storage. 2018;18:421-434. doi:https://doi.org/10.1016/j.est.2018.06.003

[62]   Lewerenz M, Dechent P, Sauer DU. Investigation of capacity recovery during rest period at different states-of-charge after cycle life test for prismatic Li(Ni1/3Mn1/3Co1/3)O2-graphite cells. J Energy Storage. 2019;21:680-690. doi:https://doi.org/10.1016/j.est.2019.01.004

[63]   Sieg J, Storch M, Fath J, et al. Local degradation and differential voltage analysis of aged lithium-ion pouch cells. J Energy Storage. 2020;30:101582. doi:https://doi.org/10.1016/j.est.2020.101582

[64]   Lewerenz M, Marongiu A, Warnecke A, Sauer DU. Differential voltage analysis as a tool for analyzing inhomogeneous ag-ing: A case study for LiFePO4|Graphite cylindrical cells. J Power Sources. 2017;368:57-67. doi:https://doi.org/10.1016/j.jpowsour.2017.09.059

[65]   Lewerenz M, Münnix J, Schmalstieg J, Käbitz S, Knips M, Sauer DU. Systematic aging of commercial LiFePO4|Graphite cy-lindrical cells including a theory explaining rise of capacity during aging. J Power Sources. 2017;345:254-263. doi:https://doi.org/10.1016/j.jpowsour.2017.01.133

[66]   National Centers for Environmental Information. Past-Weather in Messina , Italy, 2022. https://www.ncei.noaa.gov/access/past-weather/messina (accessed on 20-07-2022).

[67]   Pevec D, Babic J, Carvalho A, Ghiassi-Farrokhfal Y, Ketter W, Podobnik V. Electric Vehicle Range Anxiety: An Obstacle for the Personal Transportation (R)evolution? In: 2019 4th International Conference on Smart and Sustainable Technologies (SpliTech). ; 2019:1-8. doi:10.23919/SpliTech.2019.8783178

[68]   Napoli G, Micari S, Dispenza G, Andaloro L, Antonucci V, Polimeni A. Freight distribution with electric vehicles: A case study in Sicily. RES, infrastructures and vehicle routing. Transp Eng. 2021;3:100047. doi:https://doi.org/10.1016/j.treng.2021.100047